





Multipolar exchange interaction and complex order in insulating lanthanides

Naoya Iwahara ^{1,2,3,*}, Zhishuo Huang ^{2,3}, Ivo Neeffjes ^{2,4} and Liviu F. Chibotaru ^{2,†}

¹Graduate School of Engineering, Chiba University, 1-33 Yayoi-cho, Inage-ku, Chiba-shi, Chiba 263-8522, Japan

²Theory of Nanomaterials Group, KU Leuven, Celestijnenlaan 200F, B-3001 Leuven, Belgium

³Department of Chemistry, National University of Singapore, Block S8 Level 3, 3 Science Drive 3, 117543, Singapore

⁴Department of Physics, University of Helsinki, Helsinki 00014, Finland



(Received 28 August 2021; accepted 14 March 2022; published 1 April 2022)

In insulating lanthanides, unquenched orbital momentum and weak crystal-field (CF) splitting of the atomic J multiplet at lanthanide ions result in a highly ranked (multipolar) exchange interaction between them and a complex low-temperature magnetic order not fully uncovered by experiment. Explicitly correlated *ab initio* methods proved to be highly efficient for an accurate description of CF multiplets and magnetism of individual lanthanide ions in such materials. Here we extend this *ab initio* methodology and develop a first-principles microscopic theory of multipolar exchange interaction between J multiplets in f -metal compounds. The key point of the approach is a complete account of Goodenough's exchange mechanism along with traditional Anderson's superexchange and other contributions, the former being dominant in many lanthanide materials. Application of this methodology to the description of the ground-state order in the neodymium nitride with rocksalt structure reveals the multipolar nature of its ferromagnetic order. We found that the primary and secondary order parameters (of T_u and E_g symmetry, respectively) contain non-negligible J -tensorial contributions up to the ninth order. The calculated spin-wave dispersion and magnetic and thermodynamic properties show that they cannot be simulated quantitatively by confining to the ground CF multiplet on the Nd sites. Our results demonstrate that the *ab initio* approach to the low-energy Hamiltonian represents a powerful tool for the study of materials with complex magnetic order.

DOI: [10.1103/PhysRevB.105.144401](https://doi.org/10.1103/PhysRevB.105.144401)

I. INTRODUCTION

Magnetic insulators with strong spin-orbit coupling on magnetic sites often exhibit unconventional magnetic phases characterized by magnetic multipole moments. Contrary to pure spin systems, the unquenched orbital momentum renders relevant high-ranked components in the magnetic moments of the corresponding magnetic centers, resulting in unconventional magnetic orders and quantum spin liquids. Such multipolar phases can appear in lanthanide and actinide compounds [1–19], in heavy transition metal systems [20–26], and possibly in cold atom systems [27].

The multipolar order is often difficult to characterize experimentally because of the lack of response of high-rank multipoles to external perturbations. This situation, for example, has prevented us from unraveling the nature of the hidden order phase in URu₂Si₂ for a long time [6]. Another difficulty is the large number of parameters characterizing the intersite multipolar interactions. For example, the total number of independent parameters characterizing the exchange interaction between J multiplets of magnetic centers with open f -orbital shells (e.g., lanthanide ions) can be as large as 2079. In addition, the high-rank multipolar structure of magnetic centers gives rise to a complicated tensorial form of electron-lattice coupling which increases the complexity of the low-energy states [1,8,28]. From the theoretical side,

a reliable modeling of the multipolar phase also faces problems because only a few interactions are usually considered. For instance, the quadrupole ordering in CeB₆ [7] and the triakontadipole order in NpO₂ [9] have been investigated in this manner. Phenomenological approaches always encounter the following issues: (1) it is not possible to know *a priori* the dominant contribution among the multipolar interactions and (2) it is unclear what is the actual impact of the remaining part of the interactions.

The multipolar order could be, in principle, quantitatively analyzed by combining the microscopic theory and quantum chemistry approaches. Attempts to build such a connection have been undertaken in the past for various compounds [8,29–35]. Recently, a microscopic theory of the superexchange interaction between the ground atomic J multiplets has been developed for the f -metal compounds [1,36]. The developed microscopic model in combination with first-principles calculations enables us to accurately determine all multipolar interactions from several tens of input microscopic parameters. By this approach, the multipolar interactions in a family of lanthanide-radical single-molecule magnets were determined, and on this basis the relaxation path of magnetization was established [37,38]. It appears very tempting to extend this approach to the *ab initio* study of multipolar order in lanthanide-based magnetic insulators.

In lanthanides, the multiconfigurational structure of low-lying multiplets arises from a subtle competition between electrostatic and covalent effects in the crystal field (CF) of surrounding ligands [39]. While such level of treatment of the

*naoya.iwahara@gmail.com

†liviu.chibotaru@kuleuven.be

electronic structure cannot be attained by single-determinant methods like Hartree-Fock (HF) approximation or density functional theory (DFT), explicitly correlated *ab initio* post HF methods based on complete active space self-consistent field (CASSCF) [40,41] were recently found highly efficient for accurate description of CF multiplets and magnetism of lanthanide (Ln) centers in various materials [39,42,43]. This approach cannot be directly applied at the same level of accuracy to complexes and fragments with more than one Ln ion, which has hampered a straightforward derivation of low-energy Hamiltonian describing their multipolar exchange interaction. However, given a very strong localization of multiplets' wave functions at Ln centers, second-order electron transfer processes involving Ln $4f$ orbitals are sufficient for an adequate description of kinetic contribution to exchange interaction [1,36]. Such electron transfer processes between Ln $4f$ orbitals have been recently considered for the investigation of exchange interaction in Ln-radical pairs [37,38]. However, for a quantitative description of Ln-Ln exchange interaction, besides virtual electron transfer between magnetic $4f$ orbitals, it is also indispensable to take into account the electron delocalization from them to $5d$ and other empty Ln orbitals at neighbor magnetic centers, which gives rise to the Goodenough's exchange contribution.

We would like to stress the major difference between the exchange interaction in transition metal and lanthanide magnetic insulators. In the former, the usual situation is that the antiferromagnetic Anderson's superexchange is absolutely dominant when not forbidden by symmetry rules, exceeding by ca. an order of magnitude all other exchange contributions and leading, therefore, to strong antiferromagnetism. A known example in this paradigm is, e.g., the strong antiferromagnetism in La_2CuO_4 [44]. Exceptions arise when the overlap of magnetic orbitals is weak or exactly zero on symmetry grounds (Goodenough-Kanamori-Anderson rules [45–47]) and when Anderson's description of exchange interaction is not appropriate [48]. Then materials may become ferromagnetic due to dominating potential exchange and/or ligands' spin polarization mechanism in the former case and kinetic ferromagnetic superexchange in the latter case. On the contrary, in lanthanides the Goodenough's exchange mechanism is often dominant because of a much stronger hybridization of magnetic $4f$ orbitals with empty orbitals of excited Ln shells due to a strong admixture of bridging ligands' orbitals. When the geometry of the bridge and the symmetry of magnetic $4f$ orbitals favor strong orbital interaction with empty Ln orbitals, a relatively strong ferromagnetism arises due to this Goodenough's mechanism as, e.g., in the series of $\text{Dy}_n\text{Sc}_{3-n}\text{N}@C_{80}$, $n = 1, 2, 3$, complexes [49,50]. Note that this scenario is valid for Ln-Ln pairs and not for Ln-radical ones which can exhibit a very strong antiferromagnetism [37,51–54]. Along with exchange interaction, a dipolar magnetic interaction should be considered too when treating the pairs of lanthanide ions. None of the mentioned interactions can be neglected *a priori* in this case and should, therefore, be accounted for as contributions to the overall multipolar magnetic coupling. Such a comprehensive treatment of exchange contributions and multipolar magnetic interaction has never been attempted by *ab initio* methods so far.

Here we extend the *ab initio* approach proved successful for the description of mononuclear lanthanide complexes and fragments to the treatment of exchange interaction and develop on its basis a first-principles microscopic theory of multipolar magnetic coupling between J -multiplets in f -metal compounds. The key point of the approach is a complete account of Goodenough's exchange mechanism along with traditional Anderson's superexchange and other contributions.

The developed theory is applied to the investigation of the multipolar order in prototypical lanthanide magnetic insulator, neodymium nitride NdN, a member of a vast family of lanthanide nitrides exhibiting ferromagnetism with high critical (Curie) temperature of about a few tens of K [55]. The ferromagnetic transition does not change the x-ray diffraction patterns, indicating the irrelevance of electron-lattice interaction [56]. In addition, the magnetism in the entire family does not depend much on the kind of rare-earth ions, suggesting the primary role of intersite magnetic interaction rather than single-ion properties and prompting simple models for the explanation of its ferromagnetism [57]. Despite this apparent simplicity, our analysis unravels a complex magnetic order in NdN described by primary and secondary order parameters and containing non-negligible J -tensorial contributions up to the ninth order. At the same time, the first-principles theory reproduces well the known experimental data on the observed ferromagnetic phase. Finally, the fingerprints of multipolar order in the low-energy excitations and magnetic and thermodynamic properties are analyzed and explored.

II. MULTIPOLAR SUPEREXCHANGE INTERACTION

Because of a strong localization of magnetic $4f$ orbitals, the multipolar exchange interaction Hamiltonian for lanthanide magnetic insulators can be derived from a microscopic Hamiltonian within Anderson's superexchange theory [45,58]. In Sec. II A, the microscopic Hamiltonian is introduced. In Sec. II B, the local CF model is derived. Due to a strong localization of $4f$ orbitals and their weak hybridization with ligands' orbitals, the low-energy electronic states at Ln sites are well described by weakly CF split atomic J multiplets [59]. The corresponding CF operators are conveniently represented by irreducible tensor operators defined on the corresponding J multiplets, hereafter referred to as CF model. In Sec. II C, the intersite interaction model acting on the ground J multiplets on Ln sites is derived. Previous microscopic theory [36] is extended here to include the Goodenough's contribution [47,60] due to virtual electron transfers between the partially filled f and empty d and other orbitals. The derived exchange interaction is transformed into the irreducible tensor form, i.e., the multipolar exchange interaction Hamiltonian.

A. Microscopic Hamiltonian

The microscopic Hamiltonian \hat{H} for an insulating f -metal compound contains all the essential interactions. The Hamiltonian is written as

$$\hat{H} = \sum_i \hat{H}_{\text{loc}}^i + \hat{H}_C + \hat{H}_{\text{PE}} + \hat{H}_t. \quad (1)$$

The first term \hat{H}_{loc}^i contains the single f ion Hamiltonians at site i :

$$\hat{H}_{\text{loc}}^i = \hat{H}_{\text{orb}}^i + \hat{H}_C^i + \hat{H}_{\text{SO}}^i. \quad (2)$$

These terms include the orbital splittings, on-site Coulomb, and spin-orbit couplings, respectively. The other terms are intersite Coulomb (\hat{H}_C), potential exchange (\hat{H}_{PE}), and electron transfer (\hat{H}_t) interactions. The present model includes only the orbitals on magnetic centers in the spirit of Anderson's theory [45]. The relevant orbitals are partially filled f ($l_f = 3$) and empty d ($l_d = 2$) and s ($l_s = 0$) orbitals.

The explicit form of the local Hamiltonian \hat{H}_{loc}^i (2) is the following. The first term (\hat{H}_{orb}^i) includes the atomic orbital energies and the CF splitting:

$$\hat{H}_{\text{orb}}^i = \sum_{lm} (H_l^i)_{mm'} \hat{a}_{ilm\sigma}^\dagger \hat{a}_{ilm'\sigma}. \quad (3)$$

Here l and m are the quantum numbers for the atomic orbital angular momentum \hat{l}^2 and its z component \hat{l}_z , respectively, $\hat{a}_{ilm\sigma}^\dagger$ ($\hat{a}_{ilm\sigma}$) are the electron creation (annihilation) operators in the orbital lm with the component of electron spin σ ($= \pm 1/2$) on site i [61], and $(H_l^i)_{mm'}$ are the matrix elements of the one-electron Hamiltonian. The second term (\hat{H}_C^i) in Eq. (2) consists of the atomic electrostatic interaction between the electrons in the f shell and those between the f and the d or s orbitals (for concrete expressions, see Sec. II in Ref. [62]). The last term (\hat{H}_{SO}^i) of Eq. (2) is the spin-orbit coupling,

$$\hat{H}_{\text{SO}}^i = \sum_{lms\sigma\sigma'} \lambda_l(lms\sigma) \hat{l} \cdot \hat{s} |lm's\sigma'\rangle \hat{a}_{ilm\sigma}^\dagger \hat{a}_{ilm'\sigma'}, \quad (4)$$

where λ_l is the spin-orbit coupling parameter for the l orbital, $s = 1/2$ is electron spin, \hat{s} the electron spin operator, and $|lms\sigma\rangle$ are the spin-orbital decoupled states. Among the local interactions Eq. (2), only \hat{H}_{orb}^i may break the spherical symmetry of the model.

The explicit form of the intersite interactions in Eq. (1) is the following. The intersite \hat{H}_C and \hat{H}_{PE} are, respectively,

$$\hat{H}_{C/\text{PE}} = \frac{1}{2} \sum_{ij(i \neq j)} \hat{H}_{C/\text{PE}}^{ij}, \quad (5)$$

$$\begin{aligned} \hat{H}_C^{ij} = & \sum_{lm\sigma} (ilm, j'l'm' | \hat{g} | iln, j'l'n') \\ & \times \hat{a}_{ilm\sigma}^\dagger \hat{a}_{ilm\sigma} \hat{a}_{j'l'm'\sigma'}^\dagger \hat{a}_{j'l'n'\sigma'}, \end{aligned} \quad (6)$$

$$\begin{aligned} \hat{H}_{\text{PE}}^{ij} = & \sum_{lm\sigma} -(ilm, j'l'm' | \hat{g} | j'l'n', iln) \\ & \times \hat{a}_{ilm\sigma}^\dagger \hat{a}_{ilm\sigma} \hat{a}_{j'l'n'\sigma'}^\dagger \hat{a}_{j'l'm'\sigma}. \end{aligned} \quad (7)$$

Here $\sum_{lm\sigma}$ is the sum over all orbital and spin angular momenta, \hat{g} is the Coulomb interaction operator between electrons, and $(ilm, j'l'm' | \hat{g} | iln, j'l'n')$ and $(ilm, j'l'm' | \hat{g} | j'l'n', iln)$ are the matrix elements. The electron transfer interaction is expressed by

$$\hat{H}_t = \sum_{ij(i \neq j)} \sum_{lm'l'm'} t_{lm,l'm'}^{ij} \hat{a}_{ilm\sigma}^\dagger \hat{a}_{j'l'm'\sigma}, \quad (8)$$

where $t_{lm,l'm'}^{ij}$ indicate the electron transfer parameters between sites i and j .

The knowledge on the energy scales of the microscopic interactions is decisive to construct the low-energy states in Secs. II B 2 and II C. In the case of lanthanide systems, the on-site Coulomb interaction is the strongest (5–7 eV) [63], which is followed by the on-site spin-orbit coupling ($\lambda_f \approx 0.1$ eV) [59] and the $4f$ orbital splitting due to the hybridization with the environment (3) [39,64] and the electron transfer interaction parameters Eq. (8) between f shells (about 0.1–0.3 eV). The intersite Coulomb interaction Eq. (6) is expected to be a few times weaker than the on-site Coulomb interaction and the intersite potential exchange interaction Eq. (7) will be a few orders of magnitude smaller than the Coulomb interaction. The local interactions and the intersite Coulomb interaction are much stronger than the remaining intersite interactions. The situation is similar to those of actinide compounds. Therefore, the same approach applies to actinides [1], though the stronger delocalization of the $5f$ orbitals than the $4f$ orbitals weakens the intrasite interactions, while enhancing the CF and intersite interactions [59].

B. Crystal field model

In this section, the low-energy eigenstates of single f^N ions are derived, and on this basis the CF model is constructed. Among the microscopic interactions in the model Eq. (1), the eigenstates of a f^N ion are in the first place determined by the intra-atomic Coulomb interaction and then by the spin-orbit coupling. Thus, derived atomic states are weakly CF split. As mentioned above, the CF splitting of the atomic J multiplet is described through irreducible tensor operators acting in the space of this multiplet.

Throughout Sec. II B, the index for site i is omitted for simplicity.

1. Crystal-field states

The degeneracy of f^N configurations is lifted by the intra-atomic exchange (Hund) coupling in \hat{H}_C . The eigenstates of \hat{H}_C , the LS terms, are characterized by the total orbital \hat{L} and spin \hat{S} angular momenta because of the spherical symmetry of \hat{H}_C :

$$\hat{H}_C |f^N \alpha LM_L SM_S\rangle = E_C(f^N \alpha LS) |f^N \alpha LM_L SM_S\rangle. \quad (9)$$

Here L (S) is the quantum number for the orbital (spin) angular momentum, M_L (M_S) is the eigenvalue of \hat{L}_z (\hat{S}_z), α distinguishes the repeated LS terms, and $E_C(f^N \alpha LS)$ is the eigenenergy. LS -terms are $[L][S]$ -fold degenerate, where $[x] = 2x + 1$.

The LS terms are split into J multiplets by the spin-orbit coupling \hat{H}_{SO} :

$$(\hat{H}_C + \hat{H}_{\text{SO}}) |f^N \alpha JM_J\rangle = E_J(f^N \alpha J) |f^N \alpha JM_J\rangle. \quad (10)$$

Here J and M_J are, respectively, the quantum numbers for the total angular momentum operators, $\hat{J} = \hat{L} + \hat{S}$ and \hat{J}_z , and α distinguishes the repeated J multiplets, [65].

The ground J -multiplet states $|f^N \alpha JM_J\rangle$ are approximated by linear combinations of the lowest LS terms when the hybridization between the ground and the excited LS terms by

\hat{H}_{SO} can be ignored:

$$|f^N JM_J\rangle = \sum_{M_L M_S} |f^N LM_L SM_S\rangle \langle JM_J | LM_L SM_S\rangle. \quad (11)$$

Here $\langle JM_J | LM_L SM_S\rangle$ are the Clebsch-Gordan coefficients [66,67,68]. α is not written in Eq. (11) because each J appears only once. This approximation is often adequate for the description of the ground states of the lanthanide and actinide ions. Equation (11) becomes the basis for the description of the low-energy states of embedded f ion (hereafter L , S , and J stand for the angular momenta for the ground LS term and the ground J multiplet of the f -metal ion, respectively).

The ground J multiplets are slightly split by the weak hybridization between the f orbitals and the surrounding ligands. The local quantum states are obtained by solving the equation

$$(\hat{H}_{\text{loc}} + \hat{H}_{\text{int}})|f^N \nu\rangle = E(f^N \nu)|f^N \nu\rangle. \quad (12)$$

\hat{H}_{int} stands for a potential which originates from some parts of Coulomb and potential exchange interactions from the environment of the Ln ion. The splitting of the J multiplet occurs due to the low-symmetric components in \hat{H}_{orb} and \hat{H}_{int} . The low-energy CF states $|f^N \nu\rangle$ can be expressed by the linear combinations of the ground atomic J multiplet states,

$$|f^N \nu\rangle = \sum_{M_J} |f^N JM_J\rangle C_{JM_J, \nu}, \quad (13)$$

with the expansion coefficients $C_{JM_J, \nu}$ ($\nu = 0, 1, \dots, 2J$), which define a $[J]$ -dimensional unitary transformation matrix from $|f^N JM_J\rangle$ to $|f^N \nu\rangle$ states. This transformation assumes negligible mixing of the ground and excited J multiplets (J mixing), which is often fulfilled in lanthanide and actinide systems because the energy gaps between the ground and the excited J multiplets ($\gtrsim \lambda_f J$) are much larger than the CF splitting. The weakly CF split J multiplet Eq. (13) is employed in the derivation of analytical form of the exchange interaction below, whereas the not-explicitly-included effects of the J mixing are recovered at the level of derivation of model parameters from *ab initio* calculations of Ln fragments.

2. Model CF Hamiltonian

The CF Hamiltonian is derived by transforming the low-energy part of the local Hamiltonian into irreducible tensor form within the ground J multiplets [59]. The transformation consists of two steps: projection of the local Hamiltonian ($\hat{H}_{\text{loc}} + \hat{H}_{\text{int}}$) into the space of the ground atomic J multiplets,

$$\mathcal{H}_J = \{|f^N JM_J\rangle | M_J = -J, -J+1, \dots, J\rangle, \quad (14)$$

and the expansion of the Hamiltonian with the irreducible tensor operators. First, the local Hamiltonian in Eq. (12) is projected into the Hilbert space \mathcal{H}_J :

$$\hat{H}_{\text{CF}} = \hat{P}_J (\hat{H}_{\text{loc}} + \hat{H}_{\text{int}}) \hat{P}_J, \quad (15)$$

where \hat{P}_J is the projection operator into \mathcal{H}_J Eq. (14):

$$\hat{P}_J = \sum_{M_J} |f^N JM_J\rangle \langle f^N JM_J|. \quad (16)$$

This procedure entails the approximation employed in Eq. (13). Then introducing the irreducible tensor operators

[1,67,69] (see also Sec. I E in the Supplemental Material [62]) [70],

$$\hat{T}_{kq} = \sum_{M_J N_J} (-1)^{J-N_J} \langle kq | JM_J J - N_J \rangle |f^N JM_J\rangle \langle f^N JN_J|, \quad (17)$$

Eq. (15) is rewritten as

$$\hat{H}_{\text{CF}} = \sum_{kq} \mathcal{B}_{kq} \hat{T}_{kq}. \quad (18)$$

From the triangle inequality for the Clebsch-Gordan coefficients in Eq. (17), ranks k are integers satisfying

$$0 \leq k \leq 2J. \quad (19)$$

The CF parameters \mathcal{B}_{kq} are calculated as

$$\mathcal{B}_{kq} = \text{Tr}[\hat{T}_{kq}^\dagger \hat{H}_{\text{CF}}], \quad (20)$$

with \hat{H}_{CF} from Eq. (15). The trace (Tr) is on \mathcal{H}_J Eq. (14).

The symmetry properties of \hat{H}_{CF} are imprinted in \mathcal{B}_{kq} . The Hermiticity of \hat{H}_{CF} , $\hat{H}_{\text{CF}}^\dagger = \hat{H}_{\text{CF}}$, leads to

$$\mathcal{B}_{kq}^* = (-1)^q \mathcal{B}_{k-q}. \quad (21)$$

The time evenness, $\Theta \hat{H}_{\text{CF}} \Theta^{-1} = \hat{H}_{\text{CF}}$ [59], makes $\mathcal{B}_{kq} \neq 0$ if and only if

$$k \in \text{even positive integers} \quad (22)$$

under the constraint Eq. (19). If the CF Hamiltonian is given by the f -shell model, the upper bound of k becomes $\min(2J, 2I_f + 1)$. When $2J > 2I_f + 1$, as occurs in many f elements, the number of CF parameters is at most 27, i.e., much less than the number of the matrix elements of general $2J$ -dimensional Hermitian matrices. The number is further reduced when the system has spatial symmetry.

The CF Hamiltonian is sometimes expressed by the tesseral tensors introduced below instead of \hat{T}_{kq} . \hat{T}_{kq} Eq. (17) may be transformed into real and imaginary (tesseral) tensors (see Eq. (10) in Ref. [1]). For $q = 0$,

$$\hat{O}_k^0 = \hat{T}_{k0}, \quad (23)$$

and for $q > 0$,

$$\begin{aligned} \hat{O}_k^{-q} &= \frac{i}{\sqrt{2}} [-(-1)^q \hat{T}_{k-q} + \hat{T}_{kq}], \\ \hat{O}_k^q &= \frac{1}{\sqrt{2}} [\hat{T}_{k-q} + (-1)^q \hat{T}_{kq}]. \end{aligned} \quad (24)$$

In the following sections, the tesseral tensor form is sometimes used.

C. Effective intersite interaction

Starting from the microscopic Hamiltonian Eq. (1), first, the effective low-energy model is derived in Sec. II C 1. Subsequently, the low-energy model is cast into the irreducible tensor (multipolar) form (Sec. II C 2).

1. General form

The microscopic Hamiltonian Eq. (1) is transformed into an effective model on a low-energy Hilbert space,

$$\mathcal{H}_0 = \bigotimes_i \mathcal{H}_J^i, \quad (25)$$

using the Anderson's superexchange approach [45,58], which is appropriate for insulating lanthanides as mentioned above. Here $\mathcal{H}_J^i = \{|f^N J_i M_J\rangle\}$, Eq. (14). The microscopic Hamiltonian Eq. (1) is divided into the unperturbed \hat{H}_0 and perturbation \hat{V} parts:

$$\hat{H}_0 = \sum_i (\hat{H}_d^i + \hat{H}_s^i + \hat{H}_C^i + \hat{H}_{SO}^i) + \hat{H}_C^{(0)}, \quad (26)$$

$$\hat{V} = \sum_i \hat{H}_f^i + (\hat{H}_C - \hat{H}_C^{(0)}) + \hat{H}_{PE} + \hat{H}_t. \quad (27)$$

Here the orbital term \hat{H}_{orb} (3) is divided into the f , d , and s terms (\hat{H}_f , \hat{H}_d , and \hat{H}_s , respectively), and $\hat{H}_C^{(0)}$ is the classical intersite Coulomb interaction $u' \hat{n}_i \hat{n}_j$, where u' is the intersite Coulomb repulsion parameter and $\hat{n}_i = \sum_{m\sigma} \hat{a}_{ifm\sigma}^\dagger \hat{a}_{ifm\sigma}$. \hat{H}_0 in Eq. (26) is defined in a form that ensures the degeneracy of its eigenvalues within \mathcal{H}_0 ,

$$\hat{H}_0 \hat{P}_0 = E_0 \hat{P}_0, \quad (28)$$

where $\hat{P}_0 = \bigotimes_i \hat{P}_J^i$ and \hat{P}_J^i is given by Eq. (16). Applying the second-order perturbation theory, the effective Hamiltonian \hat{H}_{eff} is derived (see, e.g., Chap. XVI in Ref. [71]):

$$\hat{H}_{eff} = E_0 \hat{P}_0 + \hat{P}_0 \hat{V} \hat{P}_0 + \hat{P}_0 \hat{V} \frac{\hat{Q}_0}{a} \hat{V} \hat{P}_0, \quad (29)$$

$$\frac{\hat{Q}_0}{a} = \sum_{\kappa \notin \mathcal{H}_0} \hat{P}_\kappa \frac{1}{E_0 - \hat{H}_0} \hat{P}_\kappa. \quad (30)$$

Here κ denotes quantum states not included in \mathcal{H}_0 , i.e., excited (nonmagnetic) f^N states on Ln sites and one-electron transferred states. Substituting \hat{H}_0 Eq. (26) and \hat{V} Eq. (27) into \hat{H}_{eff} Eq. (29), the following form of the effective Hamiltonian is derived:

$$\hat{H}_{eff} = \hat{H}_{CF} + \Delta \hat{H}_C + \Delta \hat{H}_{PE} + \hat{H}_{KE}. \quad (31)$$

Here $\hat{H}_{CF} = \sum_i \hat{H}_{CF}^i$, and $\Delta \hat{H}_C$ and $\Delta \hat{H}_{PE}$ are the intersite Coulomb and exchange interactions with \hat{H}_{int} Eq. (12) subtracted. $\Delta \hat{H}_{C/PE}$ reads as $\hat{P}_0 \Delta \hat{H}_{C/PE} \hat{P}_0$ [\hat{P}_0 is omitted in Eq. (31) for simplicity]. The kinetic exchange interaction \hat{H}_{KE} is given by [72]

$$\hat{H}_{KE} = \hat{P}_0 \hat{H}_t \frac{\hat{Q}_0}{a} \hat{H}_t \hat{P}_0. \quad (32)$$

This term contains the contributions from the virtual one electron transfer processes, e.g., $f^N - f^{N'} \rightarrow f^{N-1} - f^{N'} l^1 \rightarrow f^N - f^{N'}$ ($l' = f, d, s$ and $f^{N'} f^1 = f^{N'+1}$). Accordingly, the kinetic exchange interaction is divided into three terms:

$$\hat{H}_{KE} = \hat{H}_{ff} + \hat{H}_{fd} + \hat{H}_{fs}, \quad (33)$$

where $\hat{H}_{f'l'}$ stands for the term involving the electron transfer interaction between the orbitals f and l' . The first term is the standard Anderson's kinetic contribution and the last two terms are Goodenough's weak ferromagnetic contributions (see Sec. IIC2 for details).

The derived low-energy model \hat{H}_{eff} Eq. (31) is transformed into the irreducible tensor form. Following the same procedure as for \hat{H}_{CF} Eq. (18), the intersite interactions (the second, third, and fourth terms in \hat{H}_{eff}) are transformed:

$$\hat{H}_X = \frac{1}{2} \sum_{ij} \sum_{k_i q_i k_j q_j} (\mathcal{I}_X^{ij})_{k_i q_i k_j q_j} \hat{T}_{k_i q_i}^i \hat{T}_{k_j q_j}^j. \quad (34)$$

Here subscript X stands for Coulomb (C), potential exchange (PE), kinetic (KE or ff, fd, fs) contributions, and $(\mathcal{I}_X^{ij})_{k_i q_i k_j q_j}$ are the interaction parameters. Each component of \mathcal{I}_X^{ij} is calculated as [see Eq. (20)]

$$(\mathcal{I}_X^{ij})_{k_i q_i k_j q_j} = \text{Tr}_{ij} [(\hat{T}_{k_i q_i}^i \otimes \hat{T}_{k_j q_j}^j)^\dagger \hat{H}_X^{ij}], \quad (35)$$

where \hat{H}_X^{ij} is the second, third, or fourth term in Eq. (31) and the trace (Tr_{ij}) is over $\mathcal{H}_J^i \otimes \mathcal{H}_J^j$. The explicit form of Eq. (35) for different contributions is shown in Sec. IIC2 and Sec. III of the Supplemental Material [62].

The nature of \hat{H}_X is reflected in \mathcal{I}_X . The Hermiticity of \hat{H}_X gives

$$(\mathcal{I}_X^{ij})_{k_i q_i k_j q_j}^* = (-1)^{q_i + q_j} (\mathcal{I}_X^{ij})_{k_i - q_i k_j - q_j}. \quad (36)$$

The time evenness of \hat{H}_X leads to the rule that $(\mathcal{I}_X^{ij})_{k_i q_i k_j q_j}$ is nonzero if and only if

$$k_i + k_j \in \text{even positive integers} \quad (37)$$

for which Eq. (19) is fulfilled. In the case that one of the k 's is zero, the relations Eqs. (36) and (37) reduce to those for the CF parameters \mathcal{B}_X , Eqs. (21) and (22), respectively.

The interaction parameter Eq. (35) for each contribution is divided into three physically different components. The first one corresponds to the case when the ranks on both sites are zero, $\mathcal{C}^{ij} = (\mathcal{I}_X^{ij})_{0000}$. This component is a constant \mathcal{C}^{ij} within \mathcal{H}_0 . Since \hat{T}_0 is proportional to the identity operator on \mathcal{H}_J , the corresponding Eq. (35) reduces to

$$\mathcal{C}_X^{ij} = \frac{1}{[J_i][J_j]} \text{Tr}_{ij} [\hat{H}_X^{ij}]. \quad (38)$$

The second component corresponds to the terms whose rank is zero only on one site. This term reduces to CF contribution \mathcal{B}^{ij} , and hence is added to \hat{H}_{CF} (18) on site i (j) when $k_i > 0$ and $k_j = 0$ ($k_i = 0, k_j > 0$). From Eq. (35), \mathcal{B}^{ij} reads

$$(\mathcal{B}_X^{ij})_{k_i q_i} = \frac{1}{[J_j]} \text{Tr}_{ij} [(\hat{T}_{k_i q_i}^i)^\dagger \hat{H}_X^{ij}]. \quad (39)$$

The last component corresponds to \mathcal{I}_X^{ij} with $k_i, k_j > 0$. This term is the exchange contribution \mathcal{J}_X^{ij} . The sum of all contributions yields for \hat{H}_X in Eq. (34),

$$\begin{aligned} \hat{H}_X^{ij} = & \mathcal{C}_X^{ij} + \sum_{k_i q_i} (\mathcal{B}_X^{ij})_{k_i q_i} \hat{T}_{k_i q_i}^i + \sum_{k_j q_j} (\mathcal{B}_X^{ij})_{k_j q_j} \hat{T}_{k_j q_j}^j \\ & + \sum_{k_i q_i k_j q_j} (\mathcal{J}_X^{ij})_{k_i q_i k_j q_j} \hat{T}_{k_i q_i}^i \hat{T}_{k_j q_j}^j, \end{aligned} \quad (40)$$

where summations go over positive k ($1 \leq k \leq 2J$).

2. Irreducible tensor form of the Goodenough's contribution

A microscopic expression of the kinetic exchange contributions is obtained by substituting the perturbation \hat{H}_1 Eq. (8) into \hat{H}_{fd} Eq. (32). Then we distinguish two contributions (1) $f-f$, involving virtual electron transfer between $4f$ Anderson's magnetic orbitals on the two sites (Anderson's superexchange mechanism), and (2) $f-d$, involving virtual electron transfer between $4f$ magnetic and $5d$ (and other) orbitals on the two sites (Goodenough's mechanism). The derivation of these microscopic expressions (and for all other

contributions to intersite magnetic interactions) as well as of their irreducible tensor form are given in Sec. III of the Supplemental Material [62]. Here we present the results for the Goodenough's contribution only. Its microscopic evaluation was not done in the past whereas, as mentioned above, it plays a crucial role in explaining particularly the ferromagnetism of lanthanide materials.

Using only $f-d$ electron transfer terms in Eqs. (8) and (32), a microscopic form of Goodenough's contribution is obtained as follows:

$$\begin{aligned} \hat{H}_{fd}^{ij} = & \sum_{\bar{\alpha}_i \bar{J}_i} \sum_{\tilde{v}_j} \sum_{m\sigma} \sum_{m'\sigma'} \frac{-t_{fm, dm'}^{ij} t_{dn', fn}^{ji}}{U_{fd}^{i \rightarrow j} + \Delta E_i(f^{N_i-1} \bar{\alpha}_i \bar{J}_i) + \Delta E_j(f^{N_j} d^1 \tilde{v}_j)} (\hat{a}_{ifm\sigma}^\dagger \hat{P}_i(f^{N_i-1} \bar{\alpha}_i \bar{J}_i) \hat{a}_{ifn\sigma'}) (\hat{a}_{jdm'\sigma} \hat{P}_j(f^{N_j} d^1 \tilde{v}_j) \hat{a}_{jdn'\sigma'}^\dagger) \\ & + \sum_{\tilde{v}_i} \sum_{\bar{\alpha}_j \bar{J}_j} \sum_{m\sigma} \sum_{m'\sigma'} \frac{-t_{dm', fm'}^{ji} t_{fn, dn'}^{ij}}{U_{fd}^{j \rightarrow i} + \Delta E_i(f^{N_i} d^1 \tilde{v}_i) + \Delta E_j(f^{N_j-1} \bar{\alpha}_j \bar{J}_j)} (\hat{a}_{idm\sigma} \hat{P}_i(f^{N_i} d^1 \tilde{v}_i) \hat{a}_{idn\sigma'}^\dagger) (\hat{a}_{jfm'\sigma}^\dagger \hat{P}_j(f^{N_j-1} \bar{\alpha}_j \bar{J}_j) \hat{a}_{jfn'\sigma'}). \end{aligned} \quad (41)$$

\hat{H}_{fd}^{ij} is understood as an operator on \mathcal{H}_0 Eq. (25) [\hat{P}_0 in Eq. (32) is omitted for simplicity]. In the microscopic form Eq. (41), $\hat{P}(f^{N-1} \bar{\alpha} \bar{J})$ and $\hat{P}(f^N d^1 \tilde{v})$ are the local projection operators into the electronic states shown in the parentheses. The quantum numbers for the f^{N-1} and $f^N d^1$ configurations are denoted with bar and tilde, e.g., \bar{J} and \tilde{v} , respectively. $U_{fd}^{i \rightarrow j}$ in the denominator is the minimal activation energy for the virtual electron transfer processes, and $\Delta E_i(f^{N_i-1} \bar{\alpha}_i \bar{J}_i)$ and $\Delta E_j(f^{N_j} d^1 \tilde{v}_j)$ are the local excitation energies with respect to the ground energies of the corresponding electron configurations. The energies of eigenstates of $f^{N_j} d^1 \tilde{v}_j$ are approximated by atomic multiplet states $\tilde{\alpha}_j \tilde{J}_j$ when the effect of orbital splitting Eq. (3) is small compared with the J multiplet splittings, which always applies to f^{N_i-1} . On the other hand, the splitting of the $5d$ orbital is comparable to that of LS term, and hence the orbital splitting effect has to be included in the calculations of the intermediate states \tilde{v}_j .

The microscopic expression Eq. (41) is transformed into the irreducible tensor form Eq. (40). First, each of the electronic operators in the parentheses in Eq. (41) is expanded with \hat{T}_{kq}^j , and then the coefficients are simplified. The intermediate states of an $f^N d^1$ ion are expanded with the atomic J multiplets $|f^N d^1 \tilde{\alpha} \tilde{J} \tilde{M}_J\rangle$ as

$$|f^N d^1 v\rangle = \sum_{\tilde{\alpha} \tilde{J} \tilde{M}_J} |f^N d^1 \tilde{\alpha} \tilde{J} \tilde{M}_J\rangle C_{\tilde{\alpha} \tilde{J} \tilde{M}_J, \tilde{v}}. \quad (42)$$

Substituting the intermediate states Eq. (42) into \hat{H}_{fd} Eq. (41), the exchange parameters become

$$\begin{aligned} (\mathcal{I}_{fd}^{ij})_{k_i q_i k_j q_j} = & \sum_{\bar{\alpha}_i \bar{J}_i} \sum_{\tilde{v}_j} \sum_{x_i \xi_i} \sum_{y_i \eta_i} \sum_{x_j \xi_j} \sum_{y_j \eta_j} \frac{-(-1)^{k_i + \eta_i + \xi_j} \tau_{fd}^{ij}(x_i \xi_i, x_j \xi_j) (\tau_{fd}^{ij}(y_i \eta_i, y_j \eta_j))^* (k_i q_i | x_i \xi_i y_i - \eta_i)}{U_{fd}^{i \rightarrow j} + \Delta E_i(f^{N_i-1} \bar{\alpha}_i \bar{J}_i) + \Delta E_j(f^{N_j} d^1 \tilde{v}_j)} \\ & \times \tilde{\Xi}_f^i(\bar{\alpha}_i \bar{L}_i \bar{S}_i \bar{J}_i, x_i y_i k_i) \tilde{Z}_{\tilde{v}_j}^j(x_j \xi_j, y_j \eta_j, k_j q_j) + (i \leftrightarrow j), \end{aligned} \quad (43)$$

where τ_{fd} are related to the electron transfer parameters,

$$\tau_{fd}^{ij}(x_i \xi_i, x_j \xi_j) = \sum_{mm'\sigma} t_{fm, dm'}^{ij}(x_i \xi_i | l_f m \sigma)(x_j \xi_j | l_d m' \sigma). \quad (44)$$

$\tilde{\Xi}_f$ and $\tilde{Z}_{\tilde{v}}$ are related to the information on on-site quantum states:

$$\tilde{\Xi}_f^i(\bar{\alpha}_i \bar{L}_i \bar{S}_i \bar{J}_i, x_i y_i k_i) = (-1)^{J_i + \bar{J}_i} \left[\prod_{z=x_i y_i} \bar{X}_f^i(\bar{\alpha}_i \bar{L}_i \bar{S}_i \bar{J}_i, z) \right] \begin{Bmatrix} x_i & \bar{J}_i & J_i \\ J_i & k_i & y_i \end{Bmatrix}, \quad (45)$$

$$\bar{X}_f^i(\bar{\alpha}_i \bar{L}_i \bar{S}_i \bar{J}_i, x_i) = (-1)^{N_i-1} \sqrt{N_i} (f^{N_i} L_i S_i | \{f^{N_i-1}(\bar{\alpha}_i \bar{L}_i \bar{S}_i) f, L_i S_i\} \sqrt{[L_i][S_i][J_i][\bar{J}_i][x_i]}) \begin{Bmatrix} L_i & S_i & J_i \\ \bar{L}_i & \bar{S}_i & \bar{J}_i \\ l_f & s & x_i \end{Bmatrix} \quad (46)$$

and

$$\begin{aligned} \tilde{Z}_{\tilde{\nu}_j}^j(x_j \xi_j, y_j \eta_j, k_j q_j) &= \sum_{M_j' N_j'} (-1)^{J_j - M_j' - \xi'} (k_j - q_j | J_j N_j' J_j - M_j') \\ &\times \sum_{\tilde{\alpha} \tilde{J}} (-1)^{\tilde{L} + \tilde{S}} \sqrt{[\tilde{L}][\tilde{S}][\tilde{J}][J_j]} \left[\sum_{\tilde{M}_j} C_{\tilde{\alpha} \tilde{J} \tilde{M}_j, \tilde{\nu}_j}(x_j \xi_j | J_j - M_j' \tilde{J} \tilde{M}_j) \right] \begin{Bmatrix} L_j & S_j & J_j \\ \tilde{L} & \tilde{S} & \tilde{J} \\ l_d & s & x_j \end{Bmatrix} \\ &\times \sum_{\tilde{\alpha}' \tilde{J}'} (-1)^{\tilde{L}' + \tilde{S}'} \sqrt{[\tilde{L}'][\tilde{S}'][\tilde{J}'][J_j]} \left[\sum_{\tilde{M}_j'} C_{\tilde{\alpha}' \tilde{J}' \tilde{M}_j', \tilde{\nu}_j}(y_j \eta_j | J_j - N_j' \tilde{J}' \tilde{M}_j') \right] \begin{Bmatrix} L_j & S_j & J_j \\ \tilde{L}' & \tilde{S}' & \tilde{J}' \\ l_d & s & y_j \end{Bmatrix}. \end{aligned} \quad (47)$$

Here $(f^N LS \{ | f^{N-1}(\tilde{\alpha} \tilde{L} \tilde{S}) f LS \})$ are coefficients of fractional parentage (c.f.p.) [73–75,76] and $6j$ and $9j$ symbols [67] are used.

From the structure of \mathcal{I}_{fd} Eq. (43), additional constraints on the allowed ranks are derived. The ranges of the ranks k_i and k_j in the first term of \mathcal{I}_{fd} Eq. (43) become, respectively,

$$\begin{aligned} 0 \leq k_i &\leq \min[2(l_f + s), 2J_i], \\ 0 \leq k_j &\leq \min[2(l_d + s) + 2\tilde{M}, 2J_j], \end{aligned} \quad (48)$$

due to the approximation employed in the above derivation. Here \tilde{M} is the largest projection \tilde{J}_z involved in the intermediate states Eq. (42). In the second term of Eq. (43), the ranges of ranks Eqs. (48) are interchanged. In a special case of degeneracy of $5d$ orbitals, the intermediate states Eq. (42) reduce to the J multiplets $| f^N d^1 \tilde{\alpha} \tilde{J} \tilde{M}_j \rangle$, and \tilde{M} in Eqs. (48) becomes 0, and consequently, the maximum allowed rank k_j for the site j becomes 5 (when $J_j > 5/2$).

III. APPLICATION TO NEODYMIUM NITRIDE

The developed theoretical framework in combination with first-principles calculations is applied to a microscopic analysis of magnetism in NdN. The system is a ferromagnet with rocksalt structure ($Fm\bar{3}m$), where Nd ions form a face centered cubic sublattice. First, the CF Eq. (18) and multipolar exchange parameters Eq. (43) are determined. Then on their basis the multipolar magnetic order is investigated.

A. *Ab initio* CF model

The CF states of an embedded Nd ions were derived based on the *ab initio* CASSCF method (see Appendix A 1). The low-lying spin-orbit multiplets of the neodymium fragment originate from the CF splitting of the ground atomic multiplet $J = 9/2$ of Nd^{3+} ion as shown in Table I. The order of the three CF multiplets, Γ_8 ($\Gamma_8^{(2)}$), Γ_6 , and Γ_8 ($\Gamma_8^{(1)}$) agrees with the previous reports [77,78].

TABLE I. *Ab initio* energy levels E_Γ and CF parameters \mathcal{B}_k for NdN (meV).

$E_{\Gamma_8^{(2)}}$	0	\mathcal{B}_0	61.652
E_{Γ_6}	18.844	\mathcal{B}_4	-32.260
$E_{\Gamma_8^{(1)}}$	39.318	\mathcal{B}_6	-12.781
		\mathcal{B}_8	1.064

Using the *ab initio* energies and wave functions of these CF multiplets, the CF Hamiltonian \hat{H}_{CF} (18) for Nd sites was uniquely derived [42,43,79],

$$\begin{aligned} \hat{H}_{\text{CF}} &= \mathcal{B}_0 \hat{O}_0^0 + \mathcal{B}_4 \left(\hat{O}_4^0 + \sqrt{\frac{5}{7}} \hat{O}_4^4 \right) + \mathcal{B}_6 \left(\hat{O}_6^0 - \sqrt{7} \hat{O}_6^4 \right) \\ &+ \mathcal{B}_8 \left(\hat{O}_8^0 + \frac{2}{3} \sqrt{\frac{7}{11}} \hat{O}_8^4 + \frac{1}{3} \sqrt{\frac{65}{11}} \hat{O}_8^8 \right), \end{aligned} \quad (49)$$

where tesseral tensor operators Eq. (24) are used. In the present case, the transformation was done using the algorithm developed for the cubic systems [80]. The calculated CF parameters are listed in Table I. The derived CF model contains eighth-rank terms at variance to the traditional f shell model [59,81], albeit their contribution is rather small [82].

The magnetic moments in the states of the ground Γ_8 multiplet, $\langle \Gamma_8 m | \hat{\mu}_z | \Gamma_8 m \rangle$, are $\pm 0.0134 \mu_B$ for $m = \mp 3/2$ and $\mp 2.0156 \mu_B$ for $m = \mp 1/2$, respectively. They are thus obtained much smaller than the free ion's value of $g_J J = 3.27$ in μ_B . The reduction is explained by the strong admixture in the states of the ground Γ_8 multiplet of $| J, \pm M \rangle$ components with low value of angular momentum projection M :

$$\begin{aligned} |\Gamma_8, \pm \frac{3}{2}\rangle &= \pm 0.800 | J, \pm \frac{3}{2} \rangle \pm 0.600 | J, \mp \frac{5}{2} \rangle, \\ |\Gamma_8, \pm \frac{1}{2}\rangle &= \pm 0.789 | J, \pm \frac{9}{2} \rangle \mp 0.607 | J, \pm \frac{1}{2} \rangle \\ &\mp 0.096 | J, \mp \frac{7}{2} \rangle. \end{aligned} \quad (50)$$

In addition, due to relatively weak spin-orbit coupling at Nd^{3+} in comparison with other Ln^{3+} in the lanthanide row, there is a strong CF admixture of states from excited atomic J multiplets [80]. The calculated reduced magnetic moment $\approx 2 \mu_B$ agrees well with experimental saturated magnetic moment M_{sat} (Table II).

B. Band structure and tight-binding model

A tight-binding electron model ($\hat{H}_{\text{orb}} + \hat{H}_t$) in the basis of maximally localized Wannier orbitals [83,84] was derived from the DFT electronic bands around the Fermi level (see Appendix A 2). To reproduce the DFT bands with the tight-binding model (the red lines in Fig. 1), the Wannier functions of $4f$, $5d$, and $6s$ type had to be included, which was achieved by including the bands from the energy interval of $2 \div 12$ eV (Fig. 1). The energies of the derived Wannier orbitals in one unit cell are given in Table III and the electron transfer parameters in Table S5 of the Supplemental Material [62]. Among

TABLE II. Magnetic properties of NdN in the paramagnetic and ferromagnetic phases: the Curie-Weiss constant T_0 , the effective magnetic moment (M_{eff}), the Curie temperature (T_C), and the saturated magnetic moment M_{sat} . The free ion data are $M_{\text{eff}} = g_J \sqrt{J(J+1)}$ and $M_{\text{sat}} = g_J J$ with $g_J = 8/11$ and $J = 9/2$.

	Paramagnetic		Ferromagnetic	
	T_0 (K)	M_{eff} (μ_B)	T_C (K)	M_{sat} (μ_B)
Theory (present)	17.9	3.70	34.5	2.22
Free ion	-	3.62	-	3.27
Anton <i>et al.</i> [78] ^a	3 ± 4	3.6 ± 0.1	43 ± 1	1.0 ± 0.2
Olcese [97]	10	3.63		
Schobinger-Papamantellos <i>et al.</i> [56]				2.7
Busch <i>et al.</i> [98,99]	24	3.65-4.00	32	3.1
Schumacher and Wallace [100]	15	3.70	35	2.15
Veyssie <i>et al.</i> [101]	19	Free ion	27.6	2.2

^aThin film with many defects.

the calculated DFT parameters, the $4f$ orbital energy levels are less accurate (Appendix B), and we do not use them in our analysis below.

The calculated band (Fig. 1) indicates a metallic ground state despite the fact that NdN is an insulator, whereas the nature of the solution does not give significant influence on \hat{H}_t because the electron transfer parameters are basically determined by the overlap of the atomic orbitals of neighboring ions. The nature of the ground state is fully taken into consideration at the stage of the treatment of the entire model Hamiltonian. The derived transfer parameters are by several tens times smaller than Coulomb repulsion [63], clearly indicating that the ground state of our model Hamiltonian is deep in the correlated insulating phase. On this basis, the exchange interaction is derived by employing Anderson's superexchange theory [45] in the next section.

C. Multipolar kinetic exchange interactions

The multipolar magnetic interaction in NdN is investigated within the developed formalism in Sec. II using the input from the first-principles calculations. As we already men-

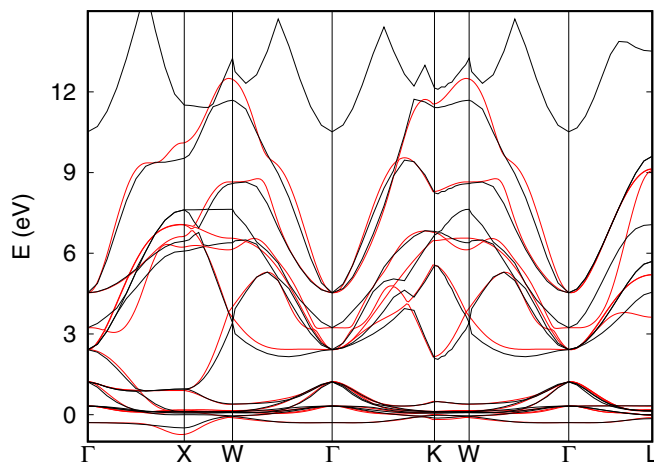


FIG. 1. Electronic band structure of NdN. Black lines correspond to DFT calculation and red lines are the result of the calculation with maximally localized Wannier functions. The Fermi level corresponds to zero energy.

tioned, the whole family of the lanthanide nitrides LnN (Ln = Nd, Sm, Gd, Tb, Dy, Ho, Er) displays ferromagnetism with close Curie temperatures (T_C) despite strong differences in the structure of the lowest multiplets of Ln^{3+} ions. The latter have less than half-filled f shells in NdN and SmN, exactly half filled in GdN, and more than half-filled in DyN and HoN [55] implying large difference in the structure of their CF multiplets. The absence of the essential difference in T_C among the LnN compounds suggests that the Goodenough's contribution \hat{H}_{fd} is dominant. In this subsection we analyze the Goodenough's exchange contribution arising from \hat{H}_{fd} in Eq. (41). The other kinetic exchange contributions and the dipolar magnetic interaction within Nd-Nd pairs are given in Sec. V of the Supplemental Material [62].

The exchange parameters \mathcal{I}_{fd} Eq. (43) were calculated by substituting the first principles data (see Sec. A) and U_{fd} into the the expressions derived in Sec. II C 2. We have chosen the values $U_{fd} = 3$ eV and 5 eV for the nearest and the next nearest neighbor Nd pairs, respectively, with which the experimental magnetic data are reproduced (see Sec. III D). These values of U_{fd} can be justified as follows. U_{fd} is roughly estimated as $U_{fd} \approx (\epsilon_d - \epsilon_f) + N(u_{fd} - u_{ff}) - u'$, where $N = 3$ is the number of $4f$ electrons in Nd^{3+} . The DFT values of the orbital energy gaps ($\epsilon_d - \epsilon_f$) between the $5d$ and the $4f$ are ca. 4.3–7.6 eV (Table III). The intra-atomic Coulomb repulsion u_{fd} is smaller than $u_{ff} \approx 5$ –7 eV [63] because of the diffuseness of the $5d$ orbitals. Indeed, the first-principles Slater-Condon fd parameters were found several times smaller than the ff ones (see Table S4 in the

TABLE III. Orbital energy levels extracted from the post HF and band calculations (eV). The irreducible representations (irrep.) of the O_h group are shown in parenthesis. The lowest post HF orbital energy level is set at zero energy.

nl	Irrep.	Post HF	DFT
$4f$	a_{2u}	0	0.0297
	t_{1u}	0.0941	0.3175
	t_{2u}	0.0191	0.2793
$5d$	t_{2g}		4.3216
	e_g		7.5913
$6s$	a_{1g}		8.6130

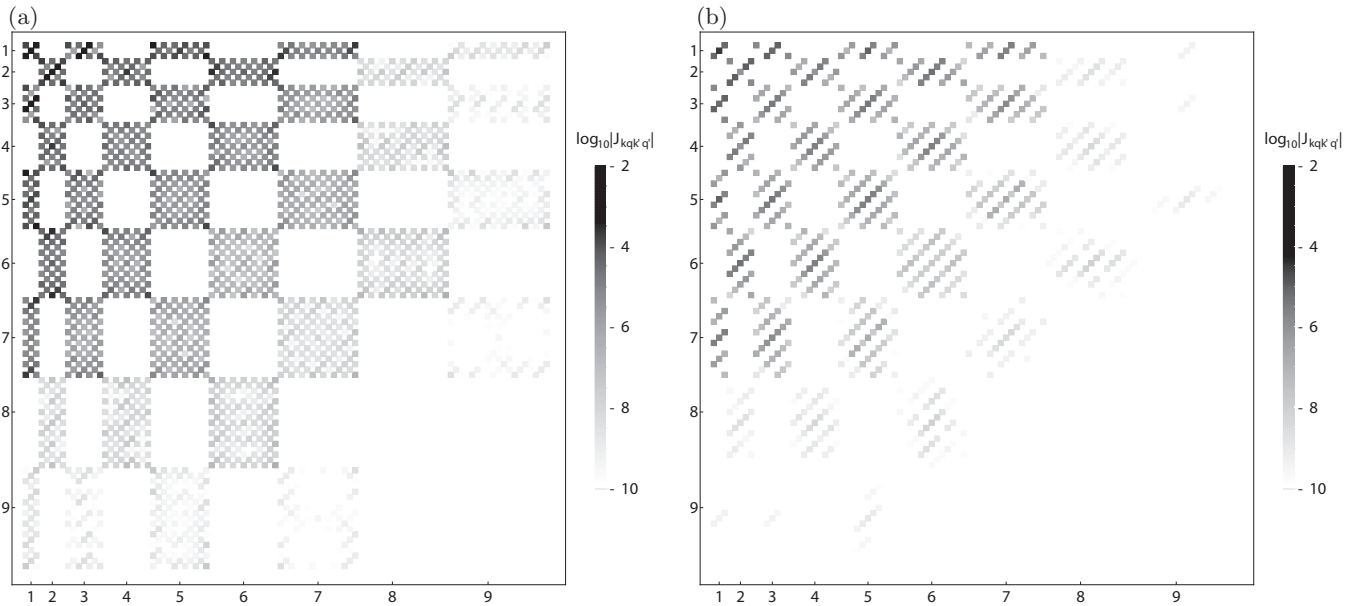


FIG. 2. Magnitude of calculated exchange parameters $(\mathcal{J}_{fd})_{kqk'q'}$ in the logarithmic scale ($\log_{10} |(\mathcal{J}_{fd})_{kqk'q'} / \text{meV}|$) for allowed values of kq and $k'q'$ for the nearest neighbor (a) and the next-nearest neighbor (b) Nd pairs in NdN. The (\mathcal{J}_{fd}) parameters presented here correspond to the tesseral tensor operators and are obtained by applying the transformation Eq. (24) to the corresponding parameters \mathcal{I}_{fd} in Eq. (43). The ticks are for kq in the increasing order of k and q .

Supplemental Material [62]). The intersite classical Coulomb repulsion in vacuum is estimated to be 4 eV for the nearest neighbors and 2.8 eV for the next-nearest neighbors, which are reduced few times by the screening effects. With these estimates, U_{fd} amounts to 4–6 eV or less. All components of the calculated \mathcal{J}_{fd} are shown in Fig. 2. The parameters corresponding to other exchange contributions are given in Figs. S3-S6 of the Supplemental Material [62].

It is easily seen that the range of possible ranks for nonzero exchange parameters Eqs. (48) is satisfied in the plots of Fig. 2. The maximum rank becomes 9 ($= 2J$) due to the ligand-field splitting of the $5d$ orbital levels at Nd [see Eqs. (48)] [85]. It also emerges that \mathcal{J}_{fd} are zero whenever the ranks k_i and k_j are of different parity, i.e., when Eq. (37) is not fulfilled. Figure 2 shows that actually there are more cases of $(\mathcal{J}_{fd})_{k_i q_i k_j q_j} = 0$ than those required by the parity of the ranks k_i and k_j , which is explained by the spatial symmetry of the interacting ion pair (for details, see Sec. V.A.1 in the Supplemental Material [62]). Furthermore, the nearest-neighbor pairs have twofold rotational symmetry, which gives an additional condition for nonzero $(\mathcal{J}_{fd})_{k_i q_i k_j q_j}$ that $q_i + q_j$ is even [86]. The next-nearest-neighbor pairs have fourfold rotational symmetry, resulting in the condition for finite $(\mathcal{J}_{fd})_{k_i q_i k_j q_j}$ that $q_i + q_j$ is a multiple of 4. The derived interaction parameters are consistent with these symmetry requirements as well as with the constraints imposed by Eqs. (48).

The multipolar interactions have non-negligible high-order terms. Figure 2 shows that the lower rank exchange parameters tend to be larger (darker in the figure) than the higher rank ones, whereas a vast number of the high rank exchange coupling terms are nonzero, and their sum could result in non-negligible effects. The significance of the high-order terms was examined by calculating the exchange spectrum of the pairs within models gradually including higher ranked

exchange interactions ($k = 1, 2, \dots, 9$) (Fig. 3). Besides, the kinetic contributions to the CF on Nd sites [the second and third terms in Eq. (40)] were analyzed in the same manner. The exchange splitting shows that the first rank contribution ($k_i = k_j = 1$) is dominant [Fig. 3(a)]. This contribution differs from an isotropic Heisenberg exchange model $2\mathcal{J}_{\text{Heis}} \hat{\mathbf{J}}_i \cdot \hat{\mathbf{J}}_j$ by several additional terms [87]. The calculated spectra display clear changes with the increase of the rank of added terms in the model up to $k = 7$ for the exchange spectrum [Fig. 3(a)] and $k = 6$ for the CF spectrum on sites [Fig. 3(b)]. This analysis suggests the importance of the high-order terms in \hat{H}_{fd} for the magnetic properties of NdN and eventually other lanthanide nitrides.

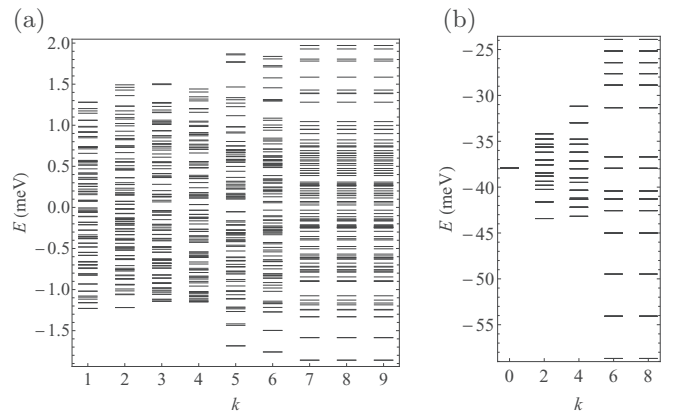


FIG. 3. The spectrum of eigenstates of the exchange (a) and CF (b) parts of the \hat{H}_{fd} operator Eq. (40) for the nearest-neighbor Nd-Nd pair. The spectrum for a given value of k corresponds to the case when terms up to k th rank are included in the corresponding operator.

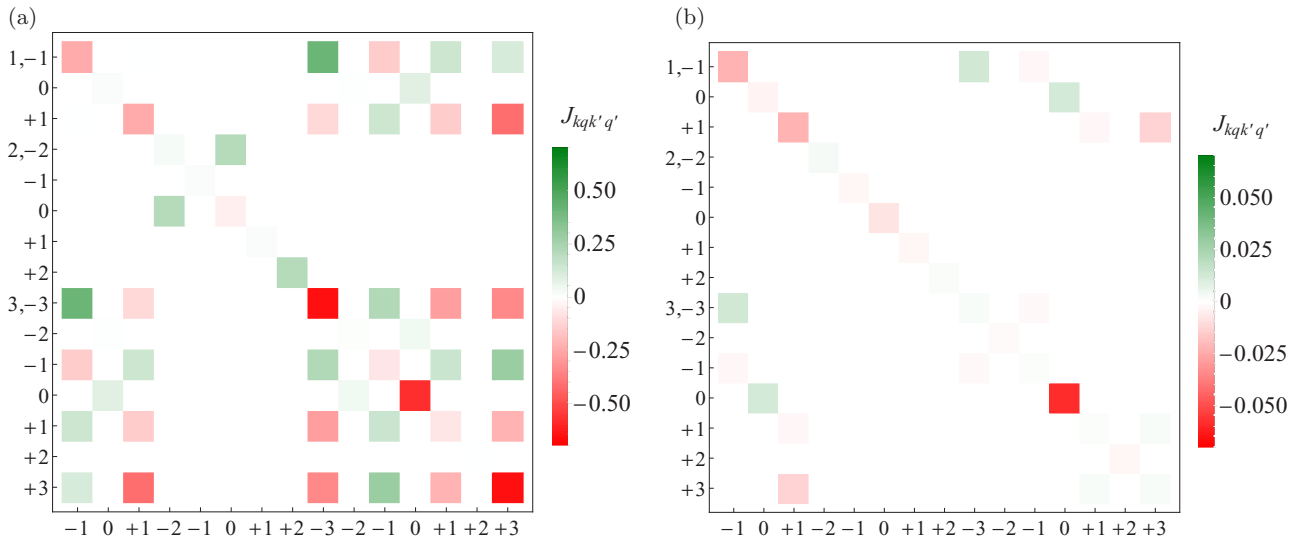


FIG. 4. The exchange parameters $(\mathcal{J}_{fd})_{kqk'q'}$ between the Γ_8 multiplets of Nd^{3+} (in meV) for the nearest (a) and the next nearest (b) neighbors. The \mathcal{J} parameters correspond to the tesseral representation of the downfolded exchange interaction between the J multiplets of the corresponding Nd pairs with exchange parameters given in Fig. 2. The red and green squares correspond to ferromagnetic and antiferromagnetic contributions.

The multipolar interactions also contribute to a scalar stabilization of the pair via the constant term \mathcal{C}_{fd} Eq. (38) in \hat{H}_{fd} (the first term in Eq. 40). The value of this term can amount to as much as ca. 10 times of the overall exchange splitting. The CF kinetic contribution described by the parameters Eq. (39) energetically is also significant [cf. Fig. 3(b)]. Again, this CF contribution is stronger than the exchange one, which becomes evident when analyzing the Goodenough's exchange mechanism [47,60]. Indeed, the expression for the exchange parameter corresponding to this mechanism contains an additional quenching factor $J_H/(U' + \Delta_{fd})$ compared to the destabilization energy of $4f$ orbitals due to f - d hybridization, $\approx t^2/(U' + \Delta_{fd})$, where t , Δ_{fd} , U' and J_H are the electron transfer parameter, the energy gap between the $4f$ and $5d$ orbitals, and intrasite Coulomb and Hund couplings, respectively.

The negligible effect of magnetic dipolar interaction in NdN (and probably in other lanthanide nitrides) is in sharp contrast with its dominant contribution to the exchange interaction in many polynuclear lanthanide complexes [88]. The Ln ions are usually found in a low-symmetric environment favoring axial CF components with respect to some quantization axis which, at its turn, stabilize a CF multiplet with a maximal projection of magnetic moment on this axis [89]. Thus, in most dysprosium complexes, the saturated magnetic moment at Dy^{3+} is $\approx 10 \mu_B$ (being, of course, highly anisotropic). Given the obtained magnetic moment on Nd^{3+} in NdN of $2.2 \mu_B$, the dipolar magnetic interaction in the former is expected to be ≈ 20 times larger than that in Nd for equal separation between Ln ions.

The evaluated exchange interaction suggests that the ferromagnetic order of NdN is of multipolar type. To obtain further physical insight, the exchange model was projected into the space of the ground Γ_8 multiplets, and transformed into the tesseral tensor form. The derived Γ_8 model shows that the strength of the nearest-neighbor interaction is about one

order of magnitude stronger than that of the next nearest-neighbor one (Fig. 4). The interactions contain both ferro- (red) and antiferromultipolar (green) contributions, the ferromagnetic contributions being overall dominant. In particular, the interactions between octupole moments ($k = 3$) are found to be the strongest. One may conclude that the exchange interaction is of ferro-octupolar type.

We have derived the multipolar exchange parameters by combining the DFT data and formula Eq. (43) rather than using other DFT based approaches because the applicability of the existing methods largely differs from that of the present method. The exchange interaction parameters have been often derived from the DFT band states by using Green's function based approach [90], which is implemented in, e.g., TB2J [91]. The approach uses one-particle Green's function constructed on top of the DFT band structure, which naturally is suitable for the description of the systems that can be well described by band states: Simple magnetic metals (Fe, Ni, Co) and alloys, and some correlated insulators SrMnO_3 , BiFeO_3 and La_2CuO_4 which could be well described within DFT+ U method with spin polarization. In these systems, the multiplet electronic structures would not play significant role. On the other hand, it is difficult to utilize the Green's function based method to study the multipolar exchange interactions of the compounds containing heavy transition metal, lanthanide, and actinide ions because in the latter systems explicit consideration of multiplet electronic structure is required.

D. Magnetic phase

With the derived multipolar interaction and CF at Nd sites, we next investigate the magnetic order of NdN within the mean-field approximation. In particular, the question on the origin of the ferromagnetism of NdN (and the entire family of lanthanide nitrides) is now addressed [92]. To establish the correct nature of the multipolar magnetic phase, the primary

order parameters should be first determined by employing the Landau theory for systems with multiple components.

The mean-field Hamiltonian for a single ion has the following form (Sec. VI.A.1 in the Supplemental Material [62]):

$$\hat{H}_{\text{MF}}^i = C_{\text{MF}}^i + \hat{H}_{\text{CF}}^i + \sum_{k_i q_i} \hat{T}_{k_i q_i}^i \mathcal{F}_{k_i q_i}^i, \quad (51)$$

where C_{MF}^i is given by

$$C_{\text{MF}}^i = -\frac{1}{2} \sum_{k_i q_i} \langle \hat{T}_{k_i q_i}^i \rangle \mathcal{F}_{k_i q_i}^i, \quad (52)$$

and the molecular field $\mathcal{F}_{k_i q_i}^i$ on site i is defined as

$$\mathcal{F}_{k_i q_i}^i = \sum_{j(\neq i)} \sum_{k_j q_j} (\mathcal{I}^{ij})_{k_i q_i k_j q_j} \langle \hat{T}_{k_j q_j}^j \rangle, \quad (53)$$

where $\langle \hat{T}_{k_i q_i}^i \rangle$ is the expectation value of the irreducible tensor operator (multipole moment) in thermal equilibrium. Diagonalizing Eq. (51), we obtain the eigenstates,

$$\hat{H}_{\text{MF}} |\mu\rangle = \epsilon_{\mu} |\mu\rangle, \quad (54)$$

where $\mu = 0, 1, \dots, 9$ and $\epsilon_0 \leq \epsilon_1 \leq \dots \leq \epsilon_9$. The mean-field solutions were obtained self-consistently so the $\langle \hat{T}_{k_i q_i}^i \rangle$ entering \hat{H}_{MF} and the ones calculated with its eigenstates $|\mu\rangle$ coincide. The most stable magnetic order was found to be the ferromagnetic one with all magnetic moments aligned along one of the crystal axes, e.g., c , in full agreement with the neutron diffraction data [56].

The stability of the calculated ferromagnetic phase was confirmed by the calculations of spin-wave dispersion. The magnon Hamiltonian was derived by employing the generalized Holstein-Primakoff transformation on top of the mean-field solutions [20,93,94] (Sec. V.A.2 in the Supplemental Material [62]). In this approach, each mean-field single-site state $|\mu\rangle$ is regarded as a one boson state, $\hat{b}_{\mu}^{\dagger}|0\rangle$, and the constraint on the number of magnon per site, $\sum_{\mu} \hat{b}_{\mu}^{\dagger} \hat{b}_{\mu} = 1$, is imposed. Using the magnon creation \hat{b}_{μ}^{\dagger} and annihilation \hat{b}_{μ} operators, the tensor operators in \hat{H}_{fd} are transformed, and the terms up to quadratic with respect to the magnon operators are retained. The obtained magnon Hamiltonian can be diagonalized by applying Bogoliubov-Valatin transformation [94–96]. The low-energy part of the calculated magnon band $\epsilon_{k\lambda}$ shows the presence of the gap between the ground and the first excited states (the black lines in Fig. 5). Therefore, the stability of the mean-field ferromagnetic solution was confirmed (for entire spin-wave spectra, see Fig. S9 in the Supplemental Material [62]). The ground state is stabilized by only 0.12 meV per site by including the zero-point energy correction.

The obtained ferromagnetic phase is characterized by non-negligible high-order multipole moments. The order parameters were derived by employing Landau theory to mean-field Helmholtz free energy. Within this approach, the second derivative of the free energy with respect to the primary order parameter becomes zero at the critical temperature. The Hessian of the mean-field free energy with respect to the multipole moments $\hat{T}_{kq}(\Gamma_8)$ defined within the ground Γ_8

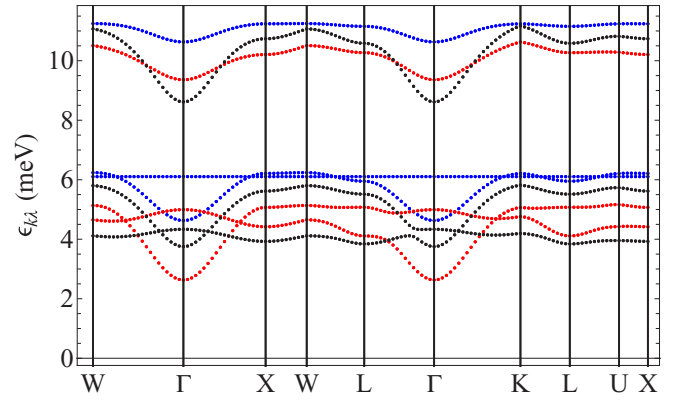


FIG. 5. Low-energy part of the spin-wave dispersion (meV). The spectra in black, red, and blue are derived with the full multipolar model, the Γ_8 model, and the Heisenberg model, respectively.

multiplet states was calculated. One of the eigenvalues of the Hessian becomes zero at $T = 29$ K (the other eigenvalues are positive). Using the corresponding eigenvector, the primary $\phi_{T_{1u}}$ and the secondary ϕ_{E_g} order parameters were determined:

$$\phi_{T_{1u}} = 0.454 \langle \hat{T}_{10}(\Gamma_8) \rangle + 0.891 \langle \hat{T}_{30}(\Gamma_8) \rangle, \quad (55)$$

$$\phi_{E_g} = \langle \hat{T}_{20}(\Gamma_8) \rangle. \quad (56)$$

The temperature evolution of the order parameters is shown in Fig. 6(a). These order parameters can be expanded through tesseral tensors \hat{O}_k^q , $\phi = \sum_{kq} c_{kq} \langle \hat{O}_k^q \rangle$ (24):

$$\begin{aligned} \phi_{T_{1u}} = & -0.316 \langle \hat{O}_1^0 \rangle - 0.313 \langle \hat{O}_3^0 \rangle + 0.026 \langle \hat{O}_5^0 \rangle \\ & + 0.228 \langle \hat{O}_5^4 \rangle - 0.257 \langle \hat{O}_7^0 \rangle + 0.534 \langle \hat{O}_7^4 \rangle \\ & - 0.517 \langle \hat{O}_9^0 \rangle - 0.355 \langle \hat{O}_9^4 \rangle + 0.075 \langle \hat{O}_9^8 \rangle, \end{aligned} \quad (57)$$

$$\begin{aligned} \phi_{E_g} = & -0.397 \langle \hat{O}_2^0 \rangle - 0.408 \langle \hat{O}_4^0 \rangle + 0.483 \langle \hat{O}_4^4 \rangle \\ & + 0.336 \langle \hat{O}_6^0 \rangle + 0.127 \langle \hat{O}_6^4 \rangle - 0.308 \langle \hat{O}_8^0 \rangle \\ & + 0.462 \langle \hat{O}_8^4 \rangle + 0.076 \langle \hat{O}_8^8 \rangle. \end{aligned} \quad (58)$$

The expectation values of the components ($c_{kq} \langle \hat{O}_k^q \rangle$) show that the largest contributions to the primary order parameter $\phi_{T_{1u}}$ come from \hat{O}_7^4 , \hat{O}_1^0 , and \hat{O}_9^0 , and those to the secondary order parameter ϕ_{E_g} are also from almost all terms [Figs. 6(d) and 6(e)]. The structures of the seventh and ninth moments are displayed in Figs. 6(b) and 6(c). This analysis indicates that the ferromagnetic phase is of nontrivial multipolar type, mainly characterized by the tensor operators of ranks 7 and 9 along with the usual rank 1.

E. Magnetic and thermodynamic quantities

The derived multipolar magnetic phase and its excitations are used for the calculation of magnetic and thermodynamic quantities of NdN (Figs. 6 and 7) (see also Sec. VI.B in the Supplemental Material [62]). These quantities include the magnetization M , magnetic susceptibility χ , magnetic entropy S_m , and the magnetic part of specific heat.

The calculated saturated magnetic moment and the Curie temperature are close to the experimental data. The

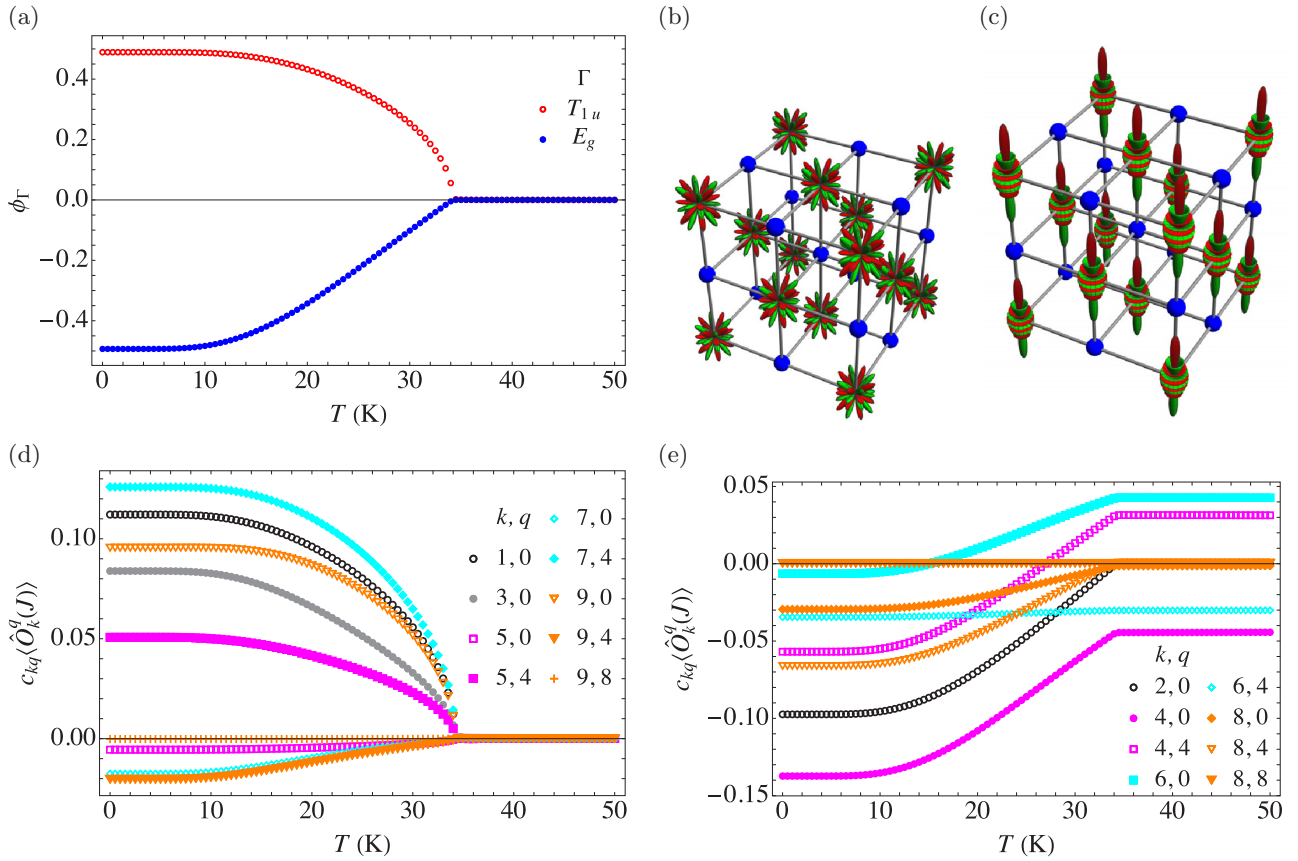


FIG. 6. Primary (T_{1u}) and secondary (E_g) order parameters (a) and the largest components in the primary order parameters (b), (c). Blue spheres are nitrogen atoms. The products of the expectation values $\langle \hat{O}_k^q \rangle$ and c_{kq} for $\phi_{T_{1u}}$ (d) and ϕ_{E_g} (e), respectively.

temperature dependence of the magnetic moment $M = \langle \hat{\mu}_z \rangle$ displays a second-order phase transition at Curie point $T_C = 34.5$ K [Fig. 7(a)]. This agrees well with experimental data [100] (see Table II) [102]. The saturated magnetic moment M_{sat} at $T = 0$ K is $2.22 \mu_B$, which is slightly enhanced by the multipolar interaction compared with the post HF value (Sec. III A). The enlargement of M_{sat} with respect to the post HF value is explained by the hybridization of the ground and excited Γ multiplets mainly due to the CF contribution in \hat{H}_{fd} (40). In terms of the local Γ multiplets [the eigenstates of the first-principles \hat{H}_{CF} Eq. (49)], the lowest four mean-field solutions $|\mu\rangle$ ($\mu = 0-3$) are written as

$$\begin{aligned}
 |0\rangle &= 0.993|\Gamma_8^{(2)}, -\frac{1}{2}\rangle + 0.076|\Gamma_6, -\frac{1}{2}\rangle \\
 &\quad - 0.087|\Gamma_8^{(1)}, -\frac{1}{2}\rangle, \\
 |1\rangle &= 0.975|\Gamma_8^{(2)}, +\frac{3}{2}\rangle - 0.223|\Gamma_8^{(1)}, +\frac{3}{2}\rangle, \\
 |2\rangle &= 1.000|\Gamma_8^{(2)}, -\frac{3}{2}\rangle + 0.018|\Gamma_8^{(1)}, -\frac{3}{2}\rangle, \\
 |3\rangle &= 0.978|\Gamma_8^{(2)}, +\frac{1}{2}\rangle + 0.136|\Gamma_6, +\frac{1}{2}\rangle \\
 &\quad - 0.157|\Gamma_8^{(1)}, +\frac{1}{2}\rangle. \quad (59)
 \end{aligned}$$

The admixture of the excited CF states in the four eigenstates Eqs. (59) are 1.3, 5.0, 0.0, and 4.3%, respectively, and the corresponding magnetic moments $\langle \hat{\mu}_z \rangle$ are 2.22, 0.67, 0.04, and $-1.60 \mu_B$.

The other calculated magnetic properties such as the Curie-Weiss constant and the effective magnetic moment also

agree well with the experimental data derived from magnetic susceptibility. Using the calculated M , the magnetic susceptibility χ was calculated [Fig. 7(b)]. The susceptibility in the high-temperature domain (80–300 K) was fit by the Curie-Weiss formula, from which the effective magnetic moment M_{eff} and the Curie-Weiss constant T_0 were extracted, $M_{\text{eff}} = 3.7 \mu_B$ and $T_0 = 18$ K. M_{eff} is close to the free ion value, suggesting that all CF multiplets contribute to the magnetic moment in the high-temperature domain. T_0 is obtained smaller than T_C , which is also in line with the experimental reports (Table II). The calculated inverse magnetic susceptibility shows a ferrimagneticlike nonlinear behavior around $35 \lesssim T \lesssim 70$ K [Fig. 7(a)], in agreement with experimental data [78]. In usual ferrimagnetic systems, the magnetic moment of a unit cell drops at the transition temperature because the magnetic moments of different sublattices partially cancel each other below T_C , while they do not in the paramagnetic phase. Similar change in magnetic moment arises in NdN too albeit by a different mechanism: the thermal population of the excited CF multiplets with large magnetic moments enhances the M_{eff} above T_C . The impact of the excited CF levels becomes visible when comparing the data with (the black lines) and without (the red lines) including them in the calculation (Fig. 7).

The calculated magnetic entropy S_m is zero at $T = 0$ K and rapidly grows as temperature rises [Fig. 7(c)]. It reaches the value of $k_B \ln 4$ at $T = T_C$, which is the entropy from the ground Γ_8 quartet, and displays a kink. Above T_C , the

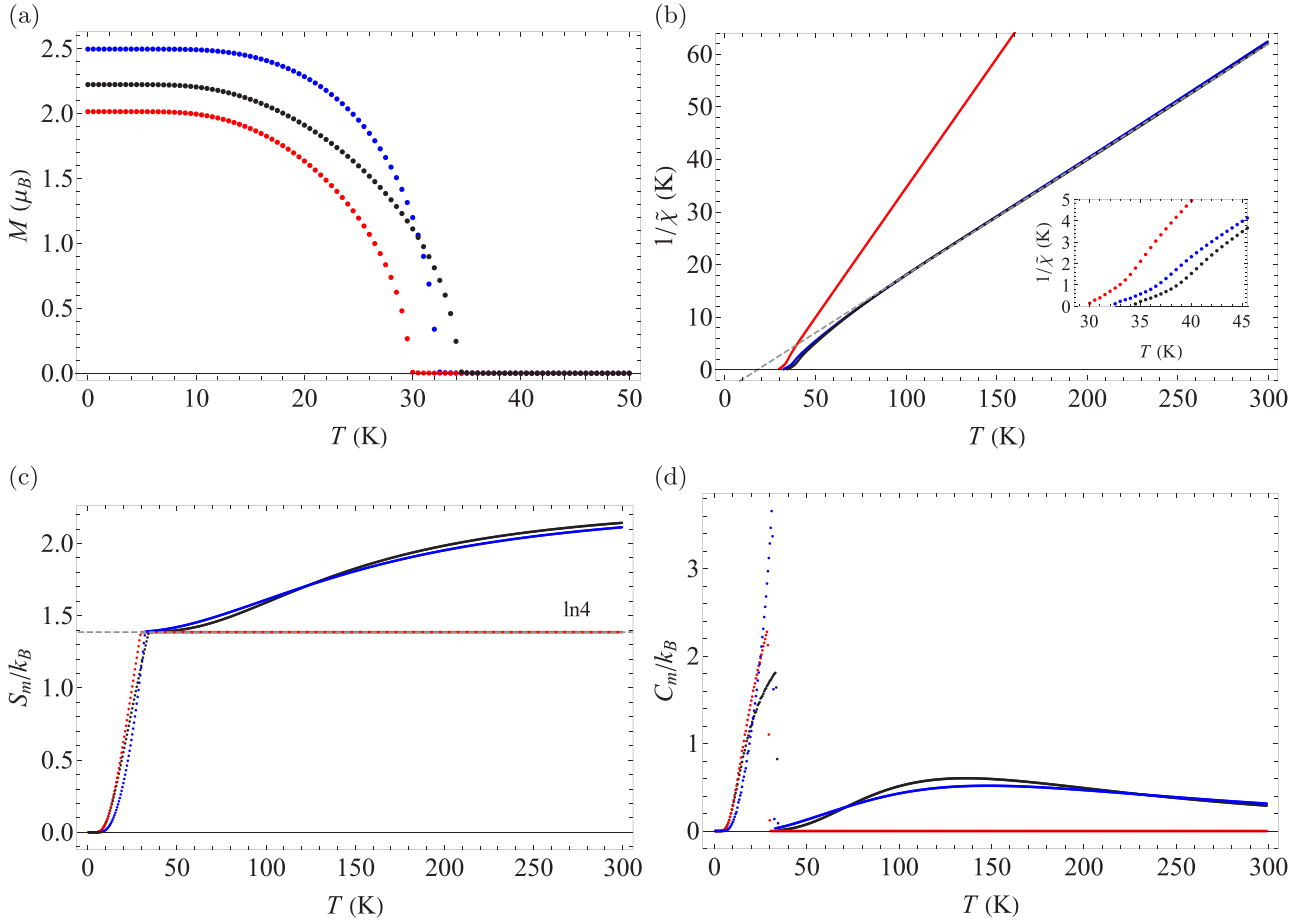


FIG. 7. Magnetic and thermodynamic properties calculated with the full multipolar model (black), the model involving only the ground Γ_8 multiplet (red), and the Heisenberg exchange model (blue). (a) Magnetization M (μ_B), (b) magnetic susceptibility $\chi = (\mu_B^2/k_B)\bar{\chi}$, (c) magnetic entropy, (d) magnetic specific heat as functions of temperature T (K). All quantities are in rapport to one unit cell.

entropy gradually increases. The magnetic part of the specific heat C_m grows from $T = 0$ K and displays a sharp peak at T_C [Fig. 7(d)]. Above T_C , C_m has a broad peak as expected from S_m . The temperature evolution of S_m and C_m above T_C is explained by the thermal population of the excited CF multiplets, similarly to M_{eff} . The importance of the excited CF multiplets for the calculated properties becomes evident from a comparison with the results of the corresponding calculations in which they are not included [red lines in Figs. 7(c) and 7(d)].

F. Fingerprint of multipolar ordering

The signs of multipolar character of the ferromagnetic phase appear in the magnon spectra. To evidence them, the magnon spectrum calculated within the multipolar exchange model was compared with the one calculated within the isotropic Heisenberg model, $2\mathcal{J}_{\text{Heis}}^ij\hat{\mathbf{J}}_i \cdot \hat{\mathbf{J}}_j$. The Heisenberg exchange parameters were chosen to match the overall exchange splitting given by the multipolar model [Fig. 3(a)], $\mathcal{J}_{\text{Heis}} = -3.51$ and -0.28 meV for the nearest- and the next-nearest-neighbor pairs, respectively. The CF Hamiltonian was kept the same as in the multipolar calculations. Figure 7 shows (blue lines) that the Heisenberg model gives similar behavior of magnetic and thermodynamic quantities with the multipole

model. Notable differences are seen in the low-energy part of the spin-wave spectrum (Fig. 5). Thus the Heisenberg magnon band (blue) at about 6 meV is flat, while the multipolar one (black) is not. Moreover, the two Heisenberg bands on X-W-L and K-L-U-X paths are quasidegenerate, while those of the multipolar model are largely split.

Hence the excitation spectra can give straightforward information on the multipolar order and interactions, however, in NdN they have not been experimentally investigated. To get insight into the multipolar order and to check the predictions given here experimental studies such as inelastic neutron scattering are most desired.

IV. CONCLUSIONS

In this paper, on the basis of explicitly correlated *ab initio* approaches and DFT calculations a first-principles microscopic theory of multipolar magnetic coupling between J -multiplets in f -electron magnetic insulators was developed. Besides conventional contributions to the exchange coupling, an important ingredient of the present theory is a complete first-principles description of Goodenough's exchange mechanism, which is of primary importance for the magnetic coupling in lanthanide materials. The theory was applied to the investigation of multipolar exchange

interaction and magnetic order in neodymium nitride. Despite the apparent simplicity of this material exhibiting a collinear ferromagnetism, our analysis reveals the multipolar nature of its magnetic order, described by primary and secondary order parameters and containing non-negligible J -tensorial contributions up to the ninth order. The first-principles theory reproduces well the known experimental data on its octupolar-ferromagnetic phase. We predict that the fingerprints of the multipolar order in this material can be found in the spin-wave dispersion and should be observable, e.g., in inelastic neutron scattering. The developed first-principles framework for the calculation of multipolar exchange parameters can become an indispensable tool in future investigations of lanthanide and actinide based magnetic insulators.

ACKNOWLEDGMENTS

N.I. was partly supported by the GOA program from KU Leuven and the scientific research Grant No. R-143-000-A80-114 of the National University of Singapore during this project. Z.H. acknowledges funding by the China Scholarship Council, the financial support of the research projects R-143-000-A65-133 and R-143-000-A80-114 of the National University of Singapore. I.N. thanks the Theoretical and Computational Chemistry European Master Program (TCCM) for financial support. The computational resources and services used in this paper were provided by the VSC (Flemish Supercomputer Center) funded by the Research Foundation-Flanders (FWO) and the Flemish Government—department EWI, as well as the one from the ASPIRE-1 cluster (www.nsc.sg) under the project 11001278.

N.I. and L.F.C. conceived this project, and designed the project. Z.H. carried out the DFT band calculations, and derived the tight-binding model. I.N. carried out the post HF calculations. N.I. developed the theoretical framework, derived the exchange model, and analyzed the magnetic phase and properties.

APPENDIX A: COMPUTATIONAL METHOD

1. Post HF calculations

The CF states of embedded Nd^{3+} were calculated employing a post-HF approach (CASSCF). To this end fragment calculations of NdN have been performed by cutting a mononuclear cluster from the experimental structure of NdN [97]. The cluster has O_h symmetry and consists of a central Nd and six nearest-neighbor N atoms which were treated fully quantum mechanically with atomic-natural orbital relativistic-correlation consistent-valence quadruple zeta polarization (ANO-RCC-VQZP) basis, and neighboring 32 N and 42 Nd with ANO-RCC-minimal basis (MB) and *ab initio* embedding model potential [103], respectively. This cluster was surrounded by 648 point charges. For the calculations of multiplet structures, CASSCF method and subsequently spin-orbit restricted-active-space state interaction (SO-RASSI) approach [40] were employed. The CASSCF/SO-RASSI calculations of the cluster were performed with three electrons in 14 active orbitals ($4f$ and $5f$ types) [104]. The atomic two-electron integrals were computed using Cholesky decomposition with a threshold of $1.0 \times 10^{-9} E_h$. The inversion

symmetry was used. All the calculations were carried out with MOLCAS 8.2 package [105].

Based on the calculated low-energy SO-RASSI states, the CF Hamiltonian was derived. By a unitary transformation of the lowest ten SO-RASSI states, the J -pseudospin states ($J = 9/2$) were uniquely defined [42,43,79]. With the obtained J pseudospin states and the energy spectrum, the first-principles based CF model [39,42,43] was derived employing the algorithm developed for O_h systems [80]. The CF parameters B_{kq} were mapped into an effective $4f$ orbital model to extract the effective orbital energy levels as in Ref. [106].

The post-HF approach was also used for isolated Nd ions to derive the Coulomb interaction (Slater-Condon) parameters and spin-orbit couplings. The CASSCF calculations of isolated Nd^{n+} ions ($n = 2-4$) were performed for all possible spin multiplicities to determine the LS -term energies. The calculated energies were fit to the electrostatic Hamiltonian for the f^N ion tabulated in Ref. [75] or those for the $f^N d^1$ or $f^N s^1$ ions [107] (see Sec. II.D in the Supplemental Material [62]). The eigenstates of the electrostatic Hamiltonian give the relation between the symmetrized LS states [75] and the LS -term states, with which the c.f.p. were transformed. The J multiplet states were obtained by performing the SO-RASSI calculations on top of the CASSCF states. By fitting the SO-RASSI levels to the model atomic Hamiltonian, the spin-orbit parameters Eq. (4) were determined (see Sec. II E in Ref. [62]).

2. DFT band calculations

The band calculations were performed with the full potential linearized augmented plane wave (LAPW) approach implemented in WIEN2K [108], allowing an accurate treatment of heavy elements. The generalized gradient approximation (GGA) functional parameterized by Perdew *et al.* [109] were employed. For the LAPW basis functions in the interstitial region, a plane-wave cutoff of $k_{\max} = 8.5/R_{\text{mt}}$ was chosen, where R_{mt} is the smallest atomic muffin-tin radius in the unit cell. The muffin-tin radii were set to $2.50 a_0$ for Nd and $2.11 a_0$ for N, where a_0 is the Bohr radius. A $6 \times 6 \times 6 k$ point sampling for Brillouin zone integral was used in the self-consistent calculation.

Based on the obtained band structure, maximally localized Wannier functions [83,84] were derived using WIEN2WANNIER [110], for which a $3 \times 3 \times 3 k$ sampling was employed. In the present case, the target bands entangle with other irrelevant bands; so to derive the Wannier functions, the strategy used in Ref. [111] was employed: This consists of including all the bands within the energy window of $[-0.5, 12.5]$ eV with an inner energy window $[-0.5, 10]$ eV (the Fermi level is set to zero of energy), and projecting the target bands onto $4f$, $5d$, and $6s$ orbitals of Nd atom. The symmetry of the obtained Wannier functions was slightly lowered, and hence they were symmetrized by comparing the obtained tight-binding model with the Slater-Koster model [112,113].

APPENDIX B: ORBITAL ENERGY LEVELS

The validity of the $4f$ orbital levels from *ab initio* and DFT calculations can be checked by making use of a relation

between the CF levels and $4f$ orbital levels. Assuming that the CF originates from single electron potential, the CF Hamiltonian \hat{H}_{CF} Eq. (18) can be mapped into a single-electron model \hat{H}_{loc} Eq. (2) and vice versa (see Sec. II B in the Supplemental Material [62]). The calculated effective orbital energy levels are given in Table III.

The $4f$ orbital energy levels derived from the post HF and DFT calculations differ significantly. The *ab initio* $4f$ orbital splitting is estimated to be only 94 meV, which is much smaller than the other intrasite interactions

Eq. (2). The order of the CF split $4f$ orbitals are consistent with the post-HF data, whereas the quantities are a few times larger than the latter. By using the same relation, we found that the DFT $4f$ orbital levels give qualitatively wrong CF levels: The calculated DFT CF levels are 0 (Γ_6), 86 (Γ_8), and 120 (Γ_8) meV. The discrepancy between DFT data and post-HF calculations could be explained by an exaggerated hybridization of the $4f$ orbitals with the ligand environment in the DFT calculations at GGA level.

-
- [1] P. Santini, S. Carretta, G. Amoretti, R. Caciuffo, N. Magnani, and G. H. Lander, Multipolar interactions in f -electron systems: The paradigm of actinide dioxides, *Rev. Mod. Phys.* **81**, 807 (2009).
- [2] Y. Kuramoto, H. Kusunose, and A. Kiss, Multipole orders and fluctuations in strongly correlated electron systems, *J. Phys. Soc. Jpn.* **78**, 072001 (2009).
- [3] T. Onimaru and H. Kusunose, Exotic quadrupolar phenomena in non-Kramers doublet systems: The cases of $\text{PrT}_2\text{Zn}_{20}$ ($T = \text{Ir, Rh}$) and $\text{PrT}_2\text{Al}_{20}$ ($T = \text{V, Ti}$), *J. Phys. Soc. Jpn.* **85**, 082002 (2016).
- [4] M.-T. Suzuki, H. Ikeda, and P. M. Oppeneer, First-principles theory of magnetic multipoles in condensed matter systems, *J. Phys. Soc. Jpn.* **87**, 041008 (2018).
- [5] J. G. Rau and M. J. Gingras, Frustrated quantum rare-earth pyrochlores, *Annu. Rev. Condens. Matter Phys.* **10**, 357 (2019).
- [6] J. A. Mydosh, P. M. Oppeneer, and P. S. Riseborough, Hidden order and beyond: An experimental—theoretical overview of the multifaceted behavior of URu_2Si_2 , *J. Phys.: Condens. Matter* **32**, 143002 (2020).
- [7] R. Shiina, H. Shiba, and P. Thalmeier, Magnetic-field effects on quadrupolar ordering in a Γ_8 -quartet system CeB_6 , *J. Phys. Soc. Jpn.* **66**, 1741 (1997).
- [8] V. S. Mironov, L. F. Chibotaru, and A. Ceulemans, First-order phase transition in UO_2 : The interplay of the $5f^2$ - $5f^2$ superexchange interaction and Jahn-Teller effect, *Adv. Quant. Chem.* **44**, 599 (2003).
- [9] P. Santini, S. Carretta, N. Magnani, G. Amoretti, and R. Caciuffo, Hidden Order and Low-Energy Excitations in NpO_2 , *Phys. Rev. Lett.* **97**, 207203 (2006).
- [10] H. Kusunose, Description of multipole in f -electron systems, *J. Phys. Soc. Jpn.* **77**, 064710 (2008).
- [11] J. G. Rau and M. J. P. Gingras, Magnitude of quantum effects in classical spin ices, *Phys. Rev. B* **92**, 144417 (2015).
- [12] H. Watanabe and Y. Yanase, Group-theoretical classification of multipole order: Emergent responses and candidate materials, *Phys. Rev. B* **98**, 245129 (2018).
- [13] J. G. Rau and M. J. P. Gingras, Frustration and anisotropic exchange in ytterbium magnets with edge-shared octahedra, *Phys. Rev. B* **98**, 054408 (2018).
- [14] S. L. Dudarev, P. Liu, D. A. Andersson, C. R. Stanek, T. Ozaki, and C. Franchini, Parametrization of LSDA + U for noncollinear magnetic configurations: Multipolar magnetism in UO_2 , *Phys. Rev. Materials* **3**, 083802 (2019).
- [15] L. V. Pourovskii and S. Khmelevskiy, Quadrupolar superexchange interactions, multipolar order, and magnetic phase transition in UO_2 , *Phys. Rev. B* **99**, 094439 (2019).
- [16] A. M. Hallas, W. Jin, J. Gaudet, E. M. Tonita, D. Pomaranski, C. R. C. Buhariwalla, M. Tachibana, N. P. Butch, S. Calder, M. B. Stone, G. M. Luke, C. R. Wiebe, J. B. Kycia, M. J. P. Gingras, and B. D. Gaulin, Intertwined magnetic dipolar and electric quadrupolar correlations in the pyrochlore $\text{Tb}_2\text{Ge}_2\text{O}_7$, [arXiv:2009.05036](https://arxiv.org/abs/2009.05036).
- [17] Y. Gritsenko, S. Mombetsu, P. T. Cong, T. Stöter, E. L. Green, C. S. Mejia, J. Wosnitza, M. Ruminy, T. Fennell, A. A. Zvyagin, S. Zherlitsyn, and M. Kenzelmann, Changes in elastic moduli as evidence for quadrupolar ordering in the rare-earth frustrated magnet $\text{Tb}_2\text{Ti}_2\text{O}_7$, *Phys. Rev. B* **102**, 060403(R) (2020).
- [18] R. Sibille, N. Gauthier, E. Lhotel, V. Porée, V. Pomjakushin, R. A. Ewings, T. G. Perring, J. Ollivier, A. Wildes, C. Ritter, T. C. Hansen, D. A. Keen, G. J. Nilsen, L. Keller, S. Petit, and T. Fennell, A quantum liquid of magnetic octupoles on the pyrochlore lattice, *Nat. Phys.* **16**, 546 (2020).
- [19] L. V. Pourovskii and S. Khmelevskiy, Hidden order and multipolar exchange striction in a correlated f -electron system, *Proc. Natl. Acad. Sci. USA* **118**, e2025317118 (2021).
- [20] G. Chen, R. Pereira, and L. Balents, Exotic phases induced by strong spin-orbit coupling in ordered double perovskites, *Phys. Rev. B* **82**, 174440 (2010).
- [21] G. Chen and L. Balents, Spin-orbit coupling in d^2 ordered double perovskites, *Phys. Rev. B* **84**, 094420 (2011).
- [22] J. Romhányi, L. Balents, and G. Jackeli, Spin-Orbit Dimers and Noncollinear Phases in d^1 Cubic Double Perovskites, *Phys. Rev. Lett.* **118**, 217202 (2017).
- [23] H. Ishikawa, T. Takayama, R. K. Kremer, J. Nuss, R. Dinnebier, K. Kitagawa, K. Ishii, and H. Takagi, Ordering of hidden multipoles in spin-orbit entangled $5d^1$ ta chlorides, *Phys. Rev. B* **100**, 045142 (2019).
- [24] D. D. Maharaj, G. Sala, M. B. Stone, E. Kermarrec, C. Ritter, F. Fauth, C. A. Marjerrison, J. E. Greedan, A. Paramakanti, and B. D. Gaulin, Octupolar Versus Néel Order in Cubic $5d^2$ Double Perovskites, *Phys. Rev. Lett.* **124**, 087206 (2020).
- [25] D. Hirai, H. Sagayama, S. Gao, H. Ohsumi, G. Chen, T. H. Arima, and Z. Hiroi, Detection of multipolar orders in the spin-orbit-coupled $5d$ Mott insulator $\text{Ba}_2\text{MgReO}_6$, *Phys. Rev. Research* **2**, 022063(R) (2020).
- [26] D. A. Wahab, M. Augustin, S. M. Valero, W. Kuang, S. Jenkins, E. Coronado, I. V. Grigorieva, I. J. Vera-Marun, E. Navarro-Moratalla, R. F. L. Evans, K. S. Novoselov, and E. J. G. Santos, Quantum rescaling, domain metastability, and hybrid domain-walls in 2D CrI_3 magnets, *Adv. Mater.* **33**, 2004138 (2021).

- [27] D. Yamamoto, C. Suzuki, G. Marmorini, S. Okazaki, and N. Furukawa, Quantum and Thermal Phase Transitions of the Triangular SU(3) Heisenberg Model under Magnetic Fields, *Phys. Rev. Lett.* **125**, 057204 (2020).
- [28] M. D. Kaplan and B. G. Vekhter, *Cooperative Phenomena in Jahn-Teller Crystals* (Plenum Press, New York, 1995).
- [29] P. M. Levy, Rare-earth-iron exchange interaction in the garnets. I. Hamiltonian for anisotropic exchange interaction, *Phys. Rev.* **135**, A155 (1964).
- [30] P. M. Levy, Rare-earth-iron exchange interaction in the garnets. II. Exchange potential for ytterbium, *Phys. Rev.* **147**, 311 (1966).
- [31] F. Hartmann-Boutron, Superexchange interactions in the presence of orbital degeneracy and spin-orbit coupling, *J. Phys. (France)* **29**, 212 (1968).
- [32] R. J. Elliott and M. F. Thorpe, Orbital effects on exchange interactions, *J. Appl. Phys.* **39**, 802 (1968).
- [33] J. M. Baker, R. J. Birgeneau, M. T. Hutchings, and J. D. Riley, High-Degree Exchange Interaction between Rare-Earth Ions, *Phys. Rev. Lett.* **21**, 620 (1968).
- [34] R. J. Birgeneau, M. T. Hutchings, J. M. Baker, and J. D. Riley, High-degree electrostatic and exchange interactions in rare-earth compounds, *J. Appl. Phys.* **40**, 1070 (1969).
- [35] V. S. Mironov, L. F. Chibotaru, and A. Ceulemans, Exchange interaction in the YbCrBr₉³⁻ mixed dimer: The origin of a strong Yb³⁺ – Cr³⁺ exchange anisotropy, *Phys. Rev. B* **67**, 014424 (2003).
- [36] N. Iwahara and L. F. Chibotaru, Exchange interaction between *J* multiplets, *Phys. Rev. B* **91**, 174438 (2015).
- [37] V. Vieru, N. Iwahara, L. Ungur, and L. F. Chibotaru, Giant exchange interaction in mixed lanthanides, *Sci. Rep.* **6**, 24046 (2016).
- [38] G. T. Nguyen and L. Ungur, Understanding the magnetization blocking mechanism in N₂³⁻-radical-bridged dilanthanide single-molecule magnets, *Phys. Chem. Chem. Phys.* **23**, 10303 (2021).
- [39] L. Ungur and L. F. Chibotaru, *Ab initio* crystal field for lanthanides, *Chem. Eur. J.* **23**, 3708 (2017).
- [40] B. O. Roos, R. Lindh, P.-A. Malmqvist, V. Veryazov, and P.-O. Widmark, *Multiconfigurational Quantum Chemistry* (John Wiley & Sons, Inc., New Jersey, 2016).
- [41] F. Aquilante, J. Autschbach, A. Baiardi, S. Battaglia, V. A. Borin, L. F. Chibotaru, I. Conti, L. De Vico, M. Delcey, I. Fdez. Galván, N. Ferré, L. Freitag, M. Garavelli, X. Gong, S. Knecht, E. D. Larsson, R. Lindh, M. Lundberg, P. Å. Malmqvist, A. Nenov *et al.*, Modern quantum chemistry with [Open]Molcas, *J. Chem. Phys.* **152**, 214117 (2020).
- [42] L. F. Chibotaru and L. Ungur, *Ab initio* calculation of anisotropic magnetic properties of complexes. I. Unique definition of pseudospin Hamiltonians and their derivation, *J. Chem. Phys.* **137**, 064112 (2012).
- [43] L. F. Chibotaru, *Ab Initio Methodology for Pseudospin Hamiltonians of Anisotropic Magnetic Complexes*, (John Wiley & Sons, Ltd., Hoboken, NJ, 2013), Chap. 6, pp. 397–519.
- [44] M. Imada, A. Fujimori, and Y. Tokura, Metal-insulator transitions, *Rev. Mod. Phys.* **70**, 1039 (1998).
- [45] P. W. Anderson, New approach to the theory of superexchange interactions, *Phys. Rev.* **115**, 2 (1959).
- [46] J. Kanamori, Superexchange interaction and symmetry properties of electron orbitals, *J. Phys. Chem. Solids* **10**, 87 (1959).
- [47] J. B. Goodenough, *Magnetism and the Chemical Bond* (Interscience, New York, 1963).
- [48] Z. Huang, D. Liu, A. Mansikkamäki, V. Vieru, N. Iwahara, and L. F. Chibotaru, Ferromagnetic kinetic exchange interaction in magnetic insulators, *Phys. Rev. Research* **2**, 033430 (2020).
- [49] V. Vieru, L. Ungur, and L. F. Chibotaru, Key role of frustration in suppression of magnetization blocking in single-molecule magnets, *J. Phys. Chem. Lett.* **4**, 3565 (2013).
- [50] R. Westerström, J. Dreiser, C. Piamonteze, M. Muntwiler, S. Weyeneth, K. Krämer, S.-X. Liu, S. Decurtins, A. Popov, S. Yang, L. Dunsch, and T. Greber, Tunneling, remanence, and frustration in dysprosium-based endohedral single-molecule magnets, *Phys. Rev. B* **89**, 060406(R) (2014).
- [51] J. D. Rinehart, M. Fang, W. J. Evans, and J. R. Long, Strong exchange and magnetic blocking in N₂³⁻-radical-bridged lanthanide complexes, *Nat. Chem.* **3**, 538 (2011).
- [52] J. D. Rinehart, M. Fang, W. J. Evans, and J. R. Long, A N₂³⁻-radical-bridged terbium complex exhibiting magnetic hysteresis at 14 K, *J. Am. Chem. Soc.* **133**, 14236 (2011).
- [53] S. Demir, M. I. Gonzalez, L. E. Darago, W. J. Evans, and J. R. Long, Giant coercivity and high magnetic blocking temperatures for N₂³⁻-radical-bridged dilanthanide complexes upon ligand dissociation, *Nat. Commun.* **8**, 2144 (2017).
- [54] C. A. P. Goodwin, B. L. L. Réant, G. F. Vettese, J. G. C. Kragsskov, M. J. Giansiracusa, I. M. DiMucci, K. M. Lancaster, D. P. Mills, and S. Sproules, Heteroleptic samarium(III) chalcogenide complexes: Opportunities for giant exchange coupling in bridging σ - and π -radical lanthanide dichalcogenides, *Inorg. Chem.* **59**, 7571 (2020).
- [55] F. Natali, B. J. Ruck, N. O. V. Plank, H. J. Trodahl, S. Granville, C. Meyer, and W. R. L. Lambrecht, Rare-earth mononitrides, *Prog. Mater. Sci.* **58**, 1316 (2013).
- [56] P. Schobinger-Papamantellos, P. Fischer, O. Vogt, and E. Kaldin, Magnetic ordering of neodymium monopnictides determined by neutron diffraction, *J. Phys. C: Solid State Phys.* **6**, 725 (1973).
- [57] T. Kasuya and D. X. Li, Mechanism of strong ferromagnetism in GdN, *J. Magn. Magn. Mater.* **167**, L1 (1997).
- [58] P. W. Anderson, Theory of magnetic exchange interactions: Exchange in insulators and semiconductors, in *Solid State Physics*, Vol. 14, edited by F. Seitz and D. Turnbull (Academic Press, New York, 1963), pp. 99–214.
- [59] A. Abragam and B. Bleaney, *Electron Paramagnetic Resonance of Transition Ions* (Clarendon Press, Oxford, 1970).
- [60] J. B. Goodenough, Theory of the role of covalence in the perovskite-type manganites [La, M(II)]MnO₃, *Phys. Rev.* **100**, 564 (1955).
- [61] The phase factor of the eigenstate of angular momentum $|jm\rangle$ ($jm = JM_J, LM_L, SM_S$) is chosen to fulfill $\Theta|jm\rangle = (-1)^{j-m}|j-m\rangle$ under time-inversion Θ [59]. This phase convention indicates that $|jm\rangle$ is expressed as $i^j Y_{jm}(\Omega)$ in (polar) coordinate representation [114] rather than the spherical harmonics $Y_{jm}(\Omega)$ with Condon-Shortley's phase convention [115], where Ω is the angular part of the three-dimensional polar coordinates. For details, see Sec. I A in Ref. [62].
- [62] See Supplemental Material at <http://link.aps.org/supplemental/10.1103/PhysRevB.105.144401> for the derivation of the exchange parameters, the first principles data, and the exchange parameters and magnetic properties of NdN. In the Supplemental Material, Refs.

- [1,10,20,36,42,43,45,48,57–59,66,67,69,71,75,79,80,93–96,107,112–129] are cited.
- [63] D. van der Marel and G. A. Sawatzky, Electron-electron interaction and localization in d and f transition metals, *Phys. Rev. B* **37**, 10674 (1988).
- [64] L. Ungur and L. F. Chibotaru, Strategies toward high-temperature lanthanide-based single-molecule magnets, *Inorg. Chem.* **55**, 10043 (2016).
- [65] α 's in Eqs. (9) and (10) are in general different from each other.
- [66] A. R. Edmonds, *Angular Momentum in Quantum Mechanics* (Princeton University Press, Princeton, 1974).
- [67] D. A. Varshalovich, A. N. Moskalev, and V. K. Khersonskii, *Quantum Theory of Angular Momentum* (World Scientific, Singapore, 1988).
- [68] The Clebsch-Gordan coefficients are chosen so they become real [66,67]. For details, see Sec. I A in Ref. [62].
- [69] K. Blum, *Density Matrix Theory and Applications*, 3rd ed. (Springer-Verlag, Berlin, 2012).
- [70] The crystal-field Hamiltonian has been traditionally represented by using Stevens operators which are expressed by polynomials of total angular momenta [59]. The irreducible tensor operators Eq. (17) have one-to-one correspondence to Stevens operators.
- [71] A. Messiah, *Quantum Mechanics* (North Holland Publishing Company, Amsterdam, 1961), Vol. II.
- [72] Only \hat{H}_i in \hat{V} is considered because the other terms do not give important contributions.
- [73] G. Racah, Theory of complex spectra. III, *Phys. Rev.* **63**, 367 (1943).
- [74] G. Racah, Theory of complex spectra. IV, *Phys. Rev.* **76**, 1352 (1949).
- [75] C. W. Nielson and G. F. Koster, *Spectroscopic Coefficients for the p^n , d^n , and f^n Configurations* (MIT Press, Cambridge, 1963).
- [76] The c.f.p.'s in Eq. (46) are defined for the atomic LS -terms Eq. (9) rather than for the symmetrized LS states tabulated in Ref. [75]. The former are obtained by a unitary transformation of the basis of the c.f.p.'s from the symmetrized states to the LS -terms.
- [77] A. Furrer, J. Kjems, and O. Vogt, Crystalline electric field levels in the neodymium monopnictides determined by neutron spectroscopy, *J. Phys. C: Solid State Phys.* **5**, 2246 (1972).
- [78] E.-M. Anton, J. F. McNulty, B. J. Ruck, M. Suzuki, M. Mizumaki, V. N. Antonov, J. W. Quilty, N. Strickland, and H. J. Trodahl, NdN: An intrinsic ferromagnetic semiconductor, *Phys. Rev. B* **93**, 064431 (2016).
- [79] L. F. Chibotaru, A. Ceulemans, and H. Bolvin, Unique Definition of the Zeeman-Splitting g Tensor of a Kramers Doublet, *Phys. Rev. Lett.* **101**, 033003 (2008).
- [80] N. Iwahara, L. Ungur, and L. F. Chibotaru, \tilde{J} -pseudospin states and the crystal field of cubic systems, *Phys. Rev. B* **98**, 054436 (2018).
- [81] K. R. Lea, M. J. M. Leask, and W. P. Wolf, The raising of angular momentum degeneracy of f -electron terms by cubic crystal fields, *J. Phys. Chem. Solids* **23**, 1381 (1962).
- [82] Without the eighth-rank terms, the CF energies become 0.1, 18.5, 39.4 meV (cf. Table I).
- [83] N. Marzari and D. Vanderbilt, Maximally localized generalized Wannier functions for composite energy bands, *Phys. Rev. B* **56**, 12847 (1997).
- [84] N. Marzari, A. A. Mostofi, J. R. Yates, I. Souza, and D. Vanderbilt, Maximally localized Wannier functions: Theory and applications, *Rev. Mod. Phys.* **84**, 1419 (2012).
- [85] Taking the atomic limit in which the $5d$ orbitals are degenerate and the eigenstates of f^3d^1 correspond to the atomic J multiplet states ($\tilde{M} \rightarrow 0$), the maximum rank for the site becomes 5 [$2(l_d + l_s)$] as expected (see Fig. S5 in the Supplemental Material [62]).
- [86] In the case of nearest-neighbor Nd pairs, like (0,0,0) and $(-1/2, -1/2, 0)$, the axis passing through the sites corresponds to a twofold rotational symmetry axis. The invariance of the exchange Hamiltonian under the π rotation around this axis allows the $(\mathcal{J}_{fd})_{k_i q_i k_j q_j}$ to be finite only for q_i and q_j with the same parity, implying that $q_i + q_j$ should be even. In the case of next-nearest-neighbor pairs, e.g., (0,0,0) and (0, 0, -1), the pair's symmetry group includes a fourfold rotational axis passing through these Nd ions. By the same argument, $(\mathcal{J}_{fd})_{k_i q_i k_j q_j}$ are finite when $q_i + q_j$ is a multiple of 4.
- [87] The energy levels of the latter are $\mathcal{J}_{\text{Heis}} J_{ij}(J_{ij} + 1)$ where J_{ij} is the total angular momentum of the $i - j$ pair ($0 \leq J_{ij} \leq 2J$).
- [88] L. F. Chibotaru, Theoretical understanding of anisotropy in molecular nanomagnets, in *Molecular Nanomagnets and Related Phenomena*, edited by S. Gao (Springer, Berlin, 2015), pp. 185–229.
- [89] L. Ungur and L. F. Chibotaru, Magnetic anisotropy in the excited states of low symmetry lanthanide complexes, *Phys. Chem. Chem. Phys.* **13**, 20086 (2011).
- [90] A. I. Liechtenstein, M. I. Katsnelson, V. P. Antropov, and V. A. Gubanov, Local spin density functional approach to the theory of exchange interactions in ferromagnetic metals and alloys, *J. Magn. Magn. Mater.* **67**, 65 (1987).
- [91] X. He, N. Helbig, M. J. Verstraete, and E. Bousquet, TB2J: A python package for computing magnetic interaction parameters, *Comput. Phys. Commun.* **264**, 107938 (2021).
- [92] Kasuya and Li proposed that the ferromagnetic interaction between two Gd ions in GdN (Gd1-N-Gd2) is determined by the third-order process of $2p$ (N) $\rightarrow 4f$ (Gd1) $\rightarrow 5d$ (Gd2) $\rightarrow 2p$ (N), in which the orbital of the bridging N atom is explicitly involved. As we show in our analysis, this contribution is a part of the Goodenough's contribution involving much more terms of equal importance. For details, see Sec. VII in the Supplemental Material [62].
- [93] A. Joshi, M. Ma, F. Mila, D. N. Shi, and F. C. Zhang, Elementary excitations in magnetically ordered systems with orbital degeneracy, *Phys. Rev. B* **60**, 6584 (1999).
- [94] H. Kusunose, *Electron Theory of Spin-Orbit Coupled-Physics* (Kodansha, Tokyo, 2019).
- [95] R. M. White, M. Sparks, and I. Ortenburger, Diagonalization of the antiferromagnetic magnon-phonon interaction, *Phys. Rev.* **139**, A450 (1965).
- [96] A. G. D. Maestro and M. J. P. Gingras, Quantum spin fluctuations in the dipolar Heisenberg-like rare earth pyrochlores, *J. Phys.: Condens. Matter* **16**, 3339 (2004).
- [97] G. L. Olcese, Interconfiguration fluctuation of cerium in CeN as a function of temperature and pressure, *J. Phys. F: Met. Phys.* **9**, 569 (1979).
- [98] G. Busch, P. Junod, F. Levy, A. Menth, and O. Vogt, Influence of crystal fields on the magnetic properties of the rare-earth nitrides, *Phys. Lett.* **14**, 264 (1965).

- [99] G. Busch, Magnetic properties of rare-earth compounds, *J. Appl. Phys.* **38**, 1386 (1967).
- [100] D. P. Schumacher and W. E. Wallace, Magnetic characteristics of some lanthanide nitrides, *Inorg. Chem.* **5**, 1563 (1966).
- [101] J. Veyssie, J. Chaussy, and A. Berton, Specific heat of lanthanum nitride and neodymium nitride, *Phys. Lett.* **13**, 29 (1964).
- [102] U_{fd} was chosen such that T_C becomes close to the experimental value.
- [103] L. Seijo and Z. Barandiarán, Computational Modelling of the Magnetic Properties of Lanthanide Compounds, in *Computational Chemistry: Reviews of Current Trends*, edited by J. Leszczynski (World Scientific, Singapore, 1999), Vol. 4, Chap. 6, pp. 55–152.
- [104] Within the post HF method, a mean-field generated by the electrons in the inactive space is considered as \hat{H}_{int} in Eq. (12).
- [105] F. Aquilante, J. Autschbach, R. K. Carlson, L. F. Chibotaru, M. G. Delcey, L. De Vico, I. Fdez. Galván, N. Ferré, L. M. Frutos, L. Gagliardi, M. Garavelli, A. Giussani, C. E. Hoyer, G. Li Manni, H. Lischka, D. Ma, P. Å. Malmqvist, T. Müller, A. Nenov, M. Olivucci *et al.*, Molcas 8: New capabilities for multiconfigurational quantum chemical calculations across the periodic table, *J. Comput. Chem.* **37**, 506 (2016).
- [106] W. Zhang, A. Muhtadi, N. Iwahara, L. Ungur, and L. F. Chibotaru, Magnetic anisotropy in divalent lanthanide compounds, *Angew. Chem., Int. Ed.* **59**, 12720 (2020).
- [107] B. R. Judd, Low-lying levels in certain actinide atoms, *Phys. Rev.* **125**, 613 (1962).
- [108] P. Blaha, K. Schwarz, G. K. H. Madsen, D. Kvasnicka, J. Luitz, R. Laskowski, F. Tran, and L. D. Marks, *WIEN2k, An Augmented Plane Wave + Local Orbitals Program for Calculating Crystal Properties* (Karlheinz Schwarz, Techn., Universität Wien, Austria, 2018).
- [109] J. P. Perdew, K. Burke, and M. Ernzerhof, Generalized Gradient Approximation Made Simple, *Phys. Rev. Lett.* **77**, 3865 (1996).
- [110] J. Kuneš, R. Arita, P. Wissgott, A. Toschi, H. Ikeda, and K. Held, Wien2wannier: From linearized augmented plane waves to maximally localized Wannier functions, *Comput. Phys. Commun.* **181**, 1888 (2010).
- [111] Y. Nomura, M. Hirayama, T. Tadano, Y. Yoshimoto, K. Nakamura, and R. Arita, Formation of a two-dimensional single-component correlated electron system and band engineering in the nickelate superconductor NdNiO₂, *Phys. Rev. B* **100**, 205138 (2019).
- [112] J. C. Slater and G. F. Koster, Simplified LCAO method for the periodic potential problem, *Phys. Rev.* **94**, 1498 (1954).
- [113] K. Takegahara, Y. Aoki, and A. Yanase, Slater-Koster tables for f electrons, *J. Phys. C: Solid State Phys.* **13**, 583 (1980).
- [114] R. Huby, Phase of matrix elements in nuclear reactions and radioactive decay, *Proc. Phys. Soc. A* **67**, 1103 (1954).
- [115] E. U. Condon and G. H. Shortley, *The Theory of Atomic Spectra* (Cambridge University Press, Cambridge, 1951).
- [116] B. R. Judd, *Second Quantization and Atomic Spectroscopy* (The Johns Hopkins Press, Baltimore, 1967).
- [117] T. Inui, Y. Tanabe, and Y. Onodera, *Group Theory and Its Applications in Physics* (Springer-Verlag, Berlin, 1990).
- [118] Wolfram Research, Inc., Mathematica, Version 12.1, Champaign, IL, 2020.
- [119] J. J. Sakurai, *Modern Quantum Mechanics*, revised ed. (Addison-Wesley, Boston, 1994).
- [120] G. Racah, Theory of complex spectra. II, *Phys. Rev.* **62**, 438 (1942).
- [121] M. Takahashi, Half-filled Hubbard model at low temperature, *J. Phys. C: Solid State Phys.* **10**, 1289 (1977).
- [122] W. Geertsma, Theory of d electrons in magnetic insulators. Long range exchange and electronic structure., Ph.D. thesis, University of Groningen, 1979.
- [123] B. E. Larson, K. C. Hass, H. Ehrenreich, and A. E. Carlsson, Exchange mechanisms in diluted magnetic semiconductors, *Solid State Commun.* **56**, 347 (1985).
- [124] J. Zaanen and G. A. Sawatzky, The electronic structure and superexchange interactions in transition-metal compounds, *Can. J. Phys.* **65**, 1262 (1987).
- [125] H. Tasaki, Ferromagnetism in Hubbard Models, *Phys. Rev. Lett.* **75**, 4678 (1995).
- [126] L. F. Chibotaru, J.-J. Girerd, G. Blondin, T. Glaser, and K. Wiegardt, Ferromagnetism and electronic delocalization in linear three nuclear complexes, in *The 5th Meeting of French Theoretical Chemists* (1996).
- [127] K. Penc, H. Shiba, F. Mila, and T. Tsukagoshi, Ferromagnetism in multiband Hubbard models: From weak to strong Coulomb repulsion, *Phys. Rev. B* **54**, 4056 (1996).
- [128] L. F. Chibotaru, J.-J. Girerd, G. Blondin, T. Glaser, and K. Wiegardt, Electronic structure of linear thiophenolate-bridged heteronuclear complexes [LFeMFeL]ⁿ⁺ (M = Cr, Co, Fe; n = 1-3): A combination of kinetic exchange interaction and electron delocalization, *J. Am. Chem. Soc.* **125**, 12615 (2003).
- [129] H. Tasaki, *Physics and Mathematics of Quantum Many-Body Systems* (Springer International Publishing, Cham, 2020).